Leipzig University of Applied Sciences
Faculty of Engineering

Program of Study:
Environmental Engineering

Bachelor Thesis

Mathematical Modelling and Analysis of a
Capillary Biofilm Reactor

written by
Zina Dhahri

Leipzig, November 2021

Supervisors: Prof. Dr.-Ing. Stephan Schönfelder
                      Leipzig University of Applied Sciences

                      M.Sc. Amelie Kenkel
                      Helmholtz Centre for Environmental Research

Erklärung

Ich versichere wahrheitsgemäß, die Bachelorarbeit selbständig angefertigt, alle benutzten Hilfsmittel vollständig und genau angegeben und alles kenntlich gemacht zu haben, was aus Arbeiten anderer unverändert oder mit Abänderungen entnommen wurde.

Bachelorarbeit Nr. 22/21

Leipzig,   November 2021

Zina Dhahri

Contents

List of Figures

List of Tables

1   Introduction

Humanity has always been striving to be better, faster and more efficient than before, this created a race against each other and time to bring forward new ideas and inventions. With an ever growing population, there also is a continuously increasing need for energy and all kinds of products, whether they are for medical, nutritional or cosmetic use. Unfortunately, the production of big quantities of fuels and chemicals for various uses has caused damage to the earth and nature. Global warming is one of the biggest consequences of draining resources and using fuels and production processes that release environmentally damaging byproducts. Therefore, it is of great importance to shift to renewable energy sources and eco-efficient processes.

Nature offers a great reservoir of resources. Energy can be produced using various sources, such as the wind, the sun, the sea etc. However, it is still a challenge to use these sources without causing further damage to the environment. Phototrophic microorganisms have the potential to produce fuels and value-added chemicals using the energy provided by the sun [3]. Due to their photosynthetic activity, they can fix carbon dioxide (CO_2), release oxygen (O_2) and provide organic carbon, which can be used for the production of various products. The replacement of fossil fuels with plant-derived fuels could contribute to the reduction of CO_2 releases. Current use of photosynthetic microorganisms ranges from human and animal nutrition to pharmaceuticals and cosmetics production [4]. One of the most promising species of these photosynthetic microorganisms are cyanobacteria, as their biomass can be further processed to produce poly-unsaturated fatty acids, antioxidants, colouring substances and fertilizers [5]. Their potential to produce hydrogen (H_2) is a field of research that has been gaining more and more attention in recent years. However, a lot of work has yet to be done in this regard [6].

In order to control their activity and retrieve the products of the biological processes, microorganisms are grown in bioreactors. For Cyanobacteria cultivation different reactor setups and formats were studied on the laboratory scale such as tubular, flat and column photobioreactors. Cells are usually grown in suspension and harvesting them by separation from the medium constitutes a challenge and accounts for 20-30 % of the production cost [7]. The research group Catalytic Biofilms at the Helmholtz Center for Environmental Research has designed a reactor setup that enables cultivation of Cyanobacteria in high cell densities and allows for continuous long-term process stabilities for at least one month: the capillary biofilm reactor. Making use of the cells natural growth behavior of forming a biofilm on the interface of solid to liquid or liquid to gaseous phases, the organisms attach to the inner wall of a capillary, while nutrients are provided via an aqueous phase constantly passing

through the capillary. Products are excreted by the cells into the medium and can be retrieved at the outlet of the reactor. This setup provides a high surface to volume ratio that ranges between $1000\text{m}^2/\text{m}^3$ to $4000\text{m}^2/\text{m}^3$ [8] and enables the cultivation of a biofilm on a large surface, resulting in large quantities of biomass, in a relatively small reactor. One major drawback of this concept is, that due to the continuous oxygen production by the phototrophic organisms, O_2 concentrations in the reactor increase over the length of the capillary. This can reach a toxic oxygen level that inhibits cell growth. For *in-situ* O_2 removal, cyanobacteria are grown in combination with oxygen respiring heterotrophic microorganisms. The reactor is therefore called a mixed species biofilm capillary reactor. The choice of the reactor material also affects the O_2 concentrations. Depending on their gas permeability, different materials contribute to the oxygen removal with different efficiencies.

As experimental methods can be time consuming and prone to error, a mathematical model of the photobioreactor could be useful for optimization and scale up. A computer simulation could deliver fast and accurate answers to questions concerning optimal feeding amounts, reactor material and length etc. It can also allow an insight into the main parts of the reactor where data cannot be collected through experimental methods without disturbing the system.

The aim of this work was the development of a time dependent model of a Mixed Species Capillary Biofilm Reactor to investigate the influence of different reactor materials on the biofilm growth and performance. The model is based on the PHO-BIA Model created by Wolf et al. in 2007. It was calibrated using experimental results from previous studies by the research group Catalytic Biofilms at the Helmholtz Center for Environmental Research. The focus of the model is on the diffusive and convective flux of oxygen, substrate and carbonate within the reactor and on the reaction kinetics of the biological conversion processes of phototrophic and heterotrophic species. The inhibitory effects of oxygen concentrations on the phototrophic growth were taken into consideration and the diffusion of O_2 through the reactor material, into the surrounding area was included. Different reactor materials and their effects on oxygen removal could be tested by changing the permeability in the model. In this work two different permeabilities and two different reactor lengths for the higher permeability were tested and the results compared to experimental results.

2 Basics

This section presents the needed information, in order to enable the reader to understand the basic biology of mixed species biofilms as well as their mathematical modeling.

2.1 Biology of Microorganisms

2.1.1 Cell Metabolism

Microorganisms can be divided into two main groups according to the carbon source they utilize: autotrophs and heterotrophs. Autotrophic organisms retrieve their carbon from CO_2, while heterotrophic organisms need organic carbon compounds like glucose [9].

Many autotrophs are phototrophic organisms, which are capable of using light energy to drive their cellular metabolism via a process called photosynthesis. Plants, algae, and Cyanobacteria perform an oxygenic photosynthesis [10]. Photosynthesis involves two main processes: energy conversion and carbon fixation. During the energy conversion process, light energy is transformed into chemical energy, whereby oxygen is released as a by-product from the water splitting reaction. The energy stored is then used in the carbon fixation process to transform carbon dioxide into organic matter [11]. Phototrophs are capable of channeling part of the carbon into internal polysaccharide reserves or into extracellular polymeric substances that are excreted in the surrounding environment [11]. In this work the focus lies on the phototrophic cyanobacteria *Synechocystis* sp. PCC 6803 (hereafter *Synechocystis*). The heterotrophic organism used is *Pseudomonas taiwanensis* VLB120 (hereafter *P. taiwanensis*).

2.1.2 Growth Inhibition

The growth of a microorganism can be decreased due to different inhibition types; competitive, non-competitive, uncompetitive, and a few others [12]. Here only the first two types will be compared. When competitive inhibition takes place, inhibitors that hamper growth compete with the substrate for the binding sites on the enzyme and a dead-end complex is formed. The inhibiting effect depends on the concentration of the substrate and the inhibitor as well as the affinity of them for the enzyme. A low substrate concentration results in a high inhibition. Therefore, the higher the substrate concentration, the lower the inhibiting effect [12]. For a phototrophic microorganism where CO_2 is a substrate, the competitive inhibition by O_2 can be

described by the term:

$$\frac{[CO_2]}{[CO_2] + \frac{K_{CO_2} \cdot [O_2]}{K_{O_2} + [O_2]}}$$
(1)

where K_i are inhibitor constants.

Non-competitive inhibitors can combine with enzyme molecules, despite the binding of substrate molecules, to produce a dead-end complex. Types of non-competitive inhibitions can be described by Michaelis-Menten-type equations. For the same phototrophic microorganism, the non-competitive inhibition by O_2 can be described by the following term:

$$\frac{K_{O_2}}{[O_2] + K_{O_2}}$$
(2)

where K_{O_2} is the O_2 inhibitor constant. This is an approach to model a non-competitive inhibition, where the reaction will never reach its normal maximum rate no matter how much substrate is available, since the enzyme is blocked by the inhibitors [13].

2.1.3 Cyanobacteria

Cyanobacteria are believed to be responsible for the oxygenation of the Earth's atmosphere. They are often referred to as Blue-Green Algae, even though they are no longer considered algae. Fig. 1 shows a microscopic image of *Synechocystis* sp. PCC 6803, a frequently used species of cyanobacteria [1]. They are a group of ecologically important phototrophic bacteria. Cyanobacteria perform oxygenic photosynthesis.

However, even though cyanobacteria produce oxygen, their growth can be hampered due to high O_2 concentrations in the reactor. Therefore, using cyanobacteria, especially *Synechocystis*, as industrial workhorse to produce value-added chemicals requires the control of oxygen concentrations to be kept below the toxic level.
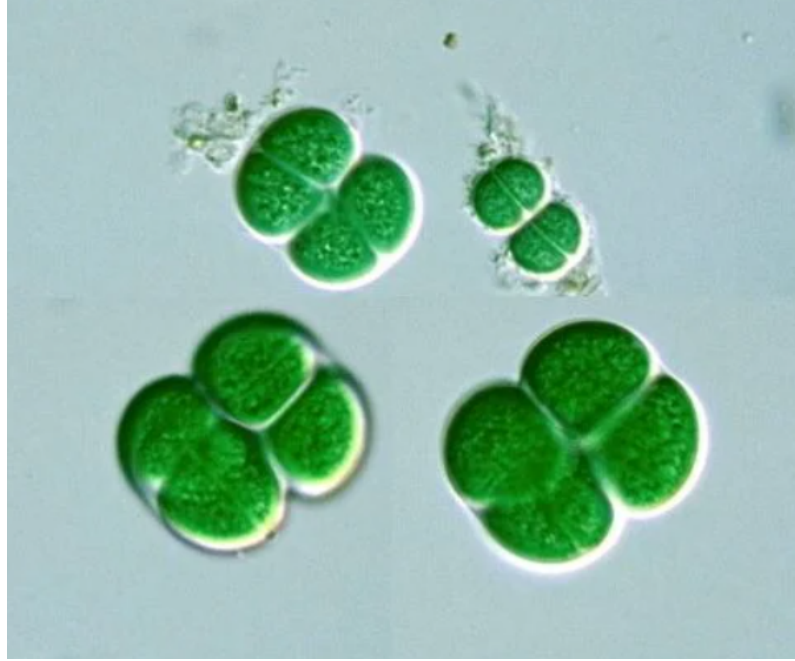
Figure 1: Microscopic image of *Synechocystis* sp. PCC 6803 [1]

2.1.4 Pseudomonas

Pseudomonads are classified as aerobes. They are oxygen respiring rod-shaped bacteria that metabolize glucose. This group contains a wide range of different species and a large metabolic diversity. Thus, they are able to grow under many conditions [14]. Fig. 2 is a Scanning Electron Microscope (SEM) image of *Pseudomonas taiwanensis* VLB 120 in a biofilm [2]. *P. taiwanensis* is known to be an excellent biofilm former and upon cocultivation with *Synechocystis*, the cyanobacterial strain is forming a stable biofilm [8]. The reason for that is not yet completely clear. One important point is the oxygen respiration by *P. taiwanensis*, which reduced O_2 concentrations in the overall system. Furthermore, *P. taiwanensis* feeds on the organic substances excreted by *Synechocystis*, thus entering a form of protocooperation.
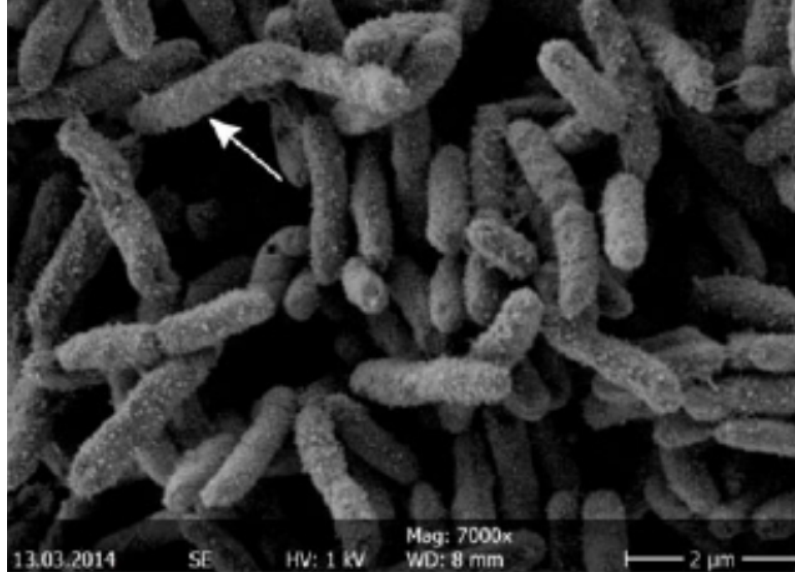
Figure 2: SEM image of *Pseudomonas taiwanensis* VLB 120 in a dehydrated biofilm [2]

2.2 Biofilms and Capillary Biofilm Reactors

2.2.1 Biofilms

Biofilms are microbial assemblages at an interface, creating a chemically distinct microenvironment, in which cells are embedded in self-produced extracellular polymeric substances (EPS). These EPS enable cellular attachment by acting as an adhesive agent [11]. Biofilms develop when conditions are favorable for microbial growth and can be found on stones in water and ship hulls, on teeth or in sewage pipelines [15]. They are robust, self-regenerative and less susceptible to chemical and mechanical stress [16, 17]. Hence, biofilm-producing bacteria pose a problem when unwanted but can be highly beneficial when grown and used in a controlled environment like a bioreactor. Biofilms can be of the pure type in which only one species grows. Or they can be of the mixed-species type, where different microorganisms are combined and benefit from each others metabolism products. Fig. 3 shows a Confocal Laser Scanning Microscopy (CLSM) image of a mixed species biofilm, where *Synechocystis* and *P. taiwanensis* were cultivated in combination [3].

In these microbial assemblages, organisms grow, consume available substrates and release products of their metabolism into the adjacent environment. A non uniform concentration distribution of dissolved species in the biofilm (such as oxygen, substrates etc.) happens due to diffusional limitations (mass transfer) and for phototrophic biofilms also due to light intensity attenuation (since the metabolism of phototrophs depends of the availability of light as energy source) [11]. Key chal-

6

lenges when applying catalytic biofilms in continuous processes include mass transfer and clogging due to excessive biomass formation [18].
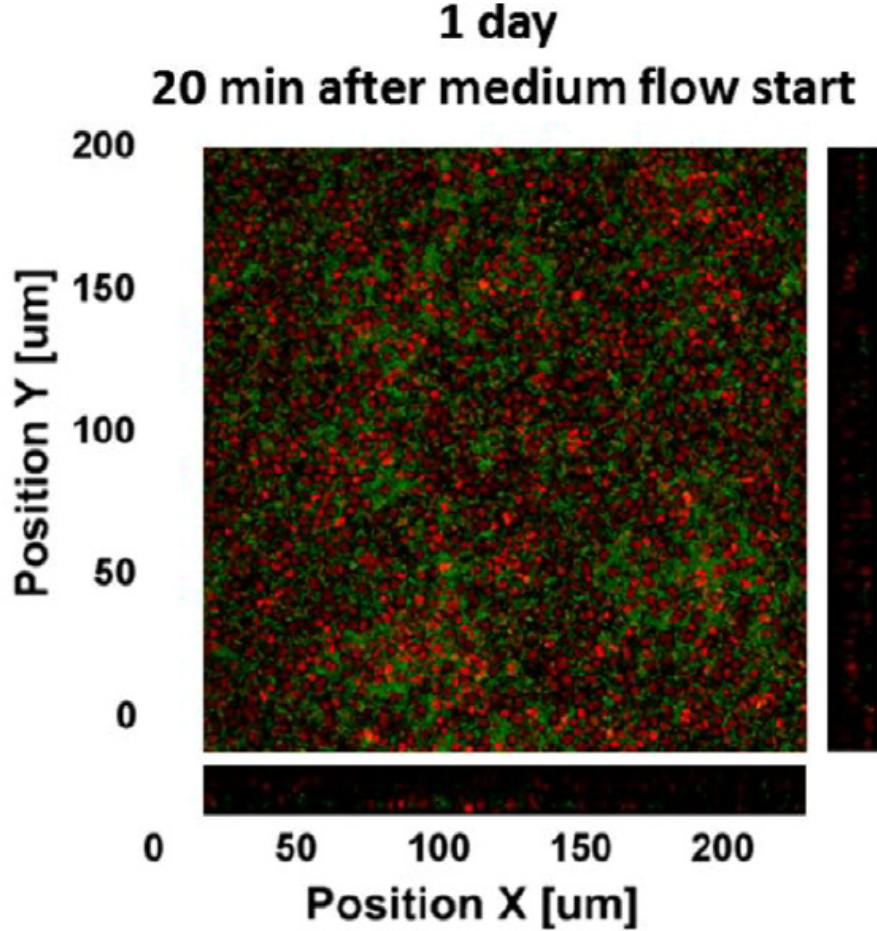
Figure 3: CLSM image of a dual-species mixed trophies biofilm. Green: *Pseudomonas taiwanensis* VLB120 with a green fluorescent protein encoding *egfp* gene integrated into its genome. Red: *Synechocystis* sp. PCC 6803 with its autofluorescent chlorophyll. [3]

2.2.2 Capillary Biofilm Reactors

Biofilm reactors have already been used in wastewater and off-gas treatment for a long time [19]. In recent years, their application field has expanded, since with the growing understanding of biofilm biology, their potential to sustainably produce chemicals and fuels is being discovered [19]. One reactor configuration to cultivate biofilms is the capillary reactor, where microorganisms are grown in an immobilized film, which is attached to the inner walls of the reactor tubes. Fig. 4, taken from Heuschkel et al. 2019, shows the setup of such a Mixed Species Capillary Biofilm Reactor. (C) is the cultivation unit. A medium flows through the capillaries from the medium bottles (A) to the waste bottles (E) and provides *Synechocystis* with the needed nutrients. Such a nutrient medium is an aqueous solution of salts and inorganic compounds. Gas accumulates in the bubble trap (D) where oxygen

concentrations can be measured. *P. taiwanensis* feeds on the organic compounds released by *Synechocystis*.

The term biomass describes the total amount of cells, and EPS in the bioreactor. To avoid clogging of the capillary tubings due to excessive biomass formation, microbial growth needs to be regulated and biofilm thickness kept under control. This could be achieved by applying hydrodynamic forces through a continuous, either single-phased or two-phased, flow. In the single-phased flow, only liquid medium is pumped through the capillaries, whereas in the two-phased plug flow, both an aqueous (medium) and a gaseous (air) phase are pumped through the capillaries. Alternating segments of air bubbles and medium can be observed in the tubes [18]. This work however focuses on the single-phase flow only.

As mentioned in the introduction, another benefit of capillary reactors is their high surface to volume ratio (1000-4000 m^2/m^3). Small tube diameters ensure a low depth of light penetration and with that an efficient light to chemical energy conversion. However, a major drawback of the cultivation of phototrophic microorganisms in biofilm capillary reactors, is the O_2 accumulation in the reactor due to oxygenic photosynthesis. High oxygen amounts inhibit cell growth [3]. Therefore, concentrations should be kept below the toxic level. *In-situ* O_2 removal can be done by co-cultivation of oxygen producing cells and oxygen respiring cells. This nature inspired cultivation of species with complementary properties, resulted in oxidative stress relief, high cell density formation and an overall more stable biofilm [3,8].
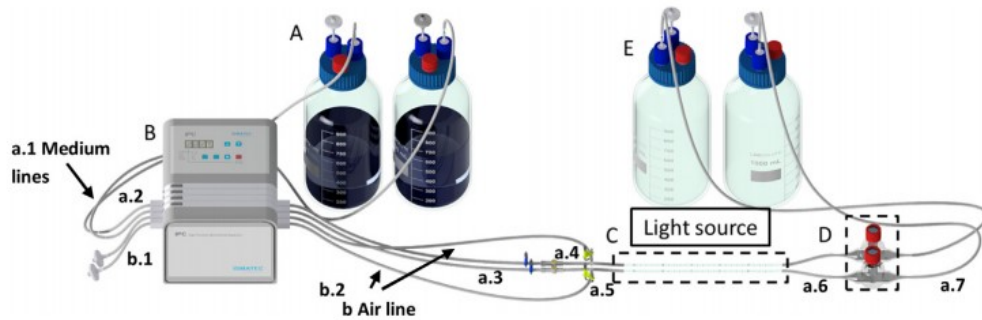
Figure 4: Biofilm capillary reactor setup. (A) Medium bottles,(B) multichannel peristaltic pump, (C) cultivation unit, (D) bubble trap, (E) Waste reservoir. Small letter indices refer to the different tubings. Figure from Heuschkel at al. 2019 [8]

2.3   Modelling Biofilms

2.3.1   Advantages, Challenges and Examples

The optimization of bioreactors can be a time consuming process. Different experiments need to be designed, prepared, conducted and evaluated. Since experimental methods are prone to error, significant and informative data can only be collected after repeating experiments several times, which makes the optimization process even longer. Modelling a system could offer a great alternative to these time consuming, expensive experimental methods. It could allow for faster and often more accurate optimization. However, one of the biggest challenges while modelling biological systems is achieving an accurate description. In nature, interactions and processes taking place in such a system are of high complexity and including all of them in a single model is almost impossible. Therefore, making the right assumptions and simplifications and including the processes that are relevant for the desired results, is a very important step in the process of developing a model.

In addition to the possibility of a faster optimization, the possibility of an insight into parts of the reactor where experimental data cannot be collected easily, also makes modelling attractive. Taking for instance the capillary reactor described in this work, the only way to collect data from inside the cultivation unit would be to interrupt the continuous cultivation and remove a part of this unit. This method disturbs the system, therefore, most data (like oxygen and carbonate concentration measurements) is collected at the inlet and/or the outlet of the cultivation unit, where sampling ports and other components can be installed. A model could give an idea about the concentrations of species like oxygen and carbonate and their distribution within this unit.

Using a computer simulation, many potential system setups and conditions can be tested and evaluated and only the most promising ones selected for further testing in a physical reactor. Realizing the advantages that computer simulations bring, many models for bioreactors were created. For example, the Activated Sludge Model (ASM1) by Henze et al. (1987) in the field of wastewater treatment [20] described a biofilm and included reactions such as carbon oxidation, nitrification and denitrification. It quantifies both the kinetics and the stoichiometry of these processes. Where the kinetics describe the rates at which reactions happen and the concentration dependence, and the stoichiometry describes the relationships between components.

The non-uniform and unpredictable structure of biofilms constitutes another challenge while modelling them [21]. Organisms often tend to form cell clusters, which lead to a porous structure. As described by C. Picioreanu et al., biofilms are het-

erogeneous in many ways, starting from the geometrical heterogeneity that includes porosity, thickness, surface coverage etc. The chemical heterogeneity manifests in the diversity of reactions, nutrients and products. The distribution of species, their diversity and activities could be classified as biological heterogeneity and biofilm viscosity, density and solute diffusivity as physical heterogeneity [21].

This huge heterogeneity makes the choice of the appropriate modelling approach, depending on the mechanisms and processes that are being investigated, one of the main tasks. Therefore, a lot of different approaches were considered to model biofilms. The IbM for example is an Individual-based Model by Kreft, Picioreanu and others, where each cell was represented by a sphere in a continuous space. Variable growth parameters were assigned to these cells. Spreading of the biomass occured by movement of the spheres to reduce the overlap between them to a minimum [15]. In the BbM (Biomass-based Model) by Picioreanu and others, distribution of biomass was assumed to be in a discrete grid. Each species had constant growth parameters [15]. In both, the IbM and the BbM, biofilm grows due to diffusion, reactions and growth processes. The two models gave similar results regarding the general growth of the biofilm, however due to the different spreading mechanisms, they differed in shape and structure [15].

2.3.2   The PHOBIA Model

This work is based on the PHOBIA Model created by Wolf et al. in 2007 [11]. The PHOBIA project had the aim to address the gap in the number of existing models that describe mixed photorophic biofilms. It is a multi-species and multi-substrate, kinetic and metabolic model, based on a one-dimensional model by Wanner and Gujer (1986) [22] and Wanner and Reichert (1996) [23]. It focuses on the interactions between photoautotrophic, heterotrophic and chemoautotrophic microorganisms. The PHOBIA model takes into consideration biological and chemical conversion processes. To develop the first stage of the model, phenomena such as light attenuation, photoinhibition and acid-base equilibria, were implemented based on planktonic models. However, since mechanisms in phototrophic biofilms are different to those in planktonic populations, a number of characteristic properties were added.

Since this work only focuses on heterotrophic and phototrophic growth and decay, as well as transformations concerning oxygen, carbonate and substrate, only the handling of these processes in the PHOBIA model will be mentioned here. The kinetic model developed in this work does not include the photoautotrophic growth under the absence of light, as the photobioreactors modeled are under the constant

influence of light. In addition to that, the mathematical description of the biological mechanisms was also inspired from the approach used by Wolf and others. Components in the model are divided into solubles and particulates. Where particulates include active and inert cells and solubles include oxygen, carbonate and substrate solved in the liquid. The stoichiometry of the reactions included in this work were based on the PHOBIA Model [11].

3   Model Development

In this section the process of developing a mathematical model for a Mixed Species Capillary Biofilm Reactor is described. The model was implemented in COMSOL Multiphysics, a simulation software based on advanced numerical methods.

Based on the PHOBIA Model, this work included the medium flow through the capillary, diffusion of oxygen, carbonate and substrate in the reactor, oxygen permeability of the reactor, the consumption and production of these components by the microorganisms and cell growth, inactivation and decay.

3.1   Assumptions and Simplifications

The number of biological processes included in the model was reduced to a minimum. The complexity of the biological system makes it almost impossible to implement all of the processes in one model. Having the goal to test different reactor materials and lengths and their impact on oxygen concentrations and with that on cell growth, the focus of this model was on diffusion mechanisms of components within and out of the reactor as well as growth, growth inhibition and decay of microorganisms. The processes included in the model are further described in section 3.2.

Being the main part of the reactor, only the cultivation unit was modeled. The geometry included was an axisymmetric tube. The reactor wall and the mass transfer mechanisms coupled to it, were simulated by adding a flux across the outer boundary of the biofilm.

The structure of the biofilm was not taken into consideration, it is assumed to be of constant maximal thickness, with a variable density, this density being the amount of cells in it. Experiments by David et al. showed that the average maximum thickness reached is $d_{bfm} = 150 \mu$m [18]. Furthermore, the biofilm was not defined as an independent material. It was assumed to be water with the addition of a correction factor to the diffusion coefficients, since diffusion in it is slower than in water. This is further explained in section 3.4.2.

3.2   Basic Biological Processes in a Biofilm Reactor

The most important part of the entire bioreactor is the cultivation unit, therefore the periphery was neglected in the model. Heterotrophic and phototrophic microorganisms are embedded within the biofilm that grows on the inside of the capillaries. The interactions between these two species and their environment as well as their

interactions among each other are very complex. Therefore, only the most fundamental processes were chosen to be included in the model. Cell growth and decay as well as the growth inhibition due to high oxygen concentrations in the reactor were included. Diffusion mechanisms of oxygen, carbonate and substrate in the reactor as well as the diffusion of oxygen out of the reactor were implemented. In addition to that, nutrient uptake and production by the microorganisms were taken into consideration. Processes concerning nitrate, phosphate and trace element consumption were not included, just like the excretion of enzymes, proteins, EPS and many other processes. Since the organic compounds released by *Synechocystis* were not included in the model, *P. taiwanensis* was assumed to feed on substrate for a first approach. Substrate is a general term that usually includes all substances (organic or inorganic) that are consumed by bacteria. In this work the term specifically refers to inert cells that slowly degrade into organic substances.

Fig. 5 schematically represents some of the basic biological processes taking place in the cultivation unit of a capillary reactor that were included in the model. Only half of the tube is represented here, this abstraction is further explained in section 3.4.1. Medium (here light blue) flows through the tube while the biofilm (here light green) is immobile, attached to the inner wall (here white). Diffusion of components (O_2, carbonate/CO_2 and substrate) is represented with white arrows. The O_2 production by phototrophs and its consumption by the heterotrophs is represented with a black arrow. The CO_2 production by heterotrophs and its consumption by the phototrophs is represented with the red arrow. In Fig. 5a only the O_2 accumulation towards the outlet of the cultivation unit was included, the geometry of the reactor material as well as the flux of oxygen across this layer was not included. The cultivation unit material is included in Fig. 5b.
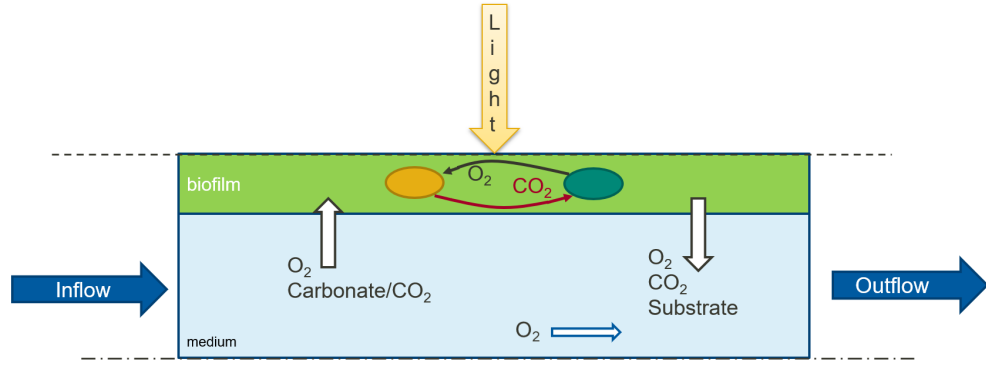
(a) Cultivation unit with omitted reactor material, no oxygen flux across the boundary between biofilm and reactor wall. O_2 accumulation towards the outlet of the cultivation unit
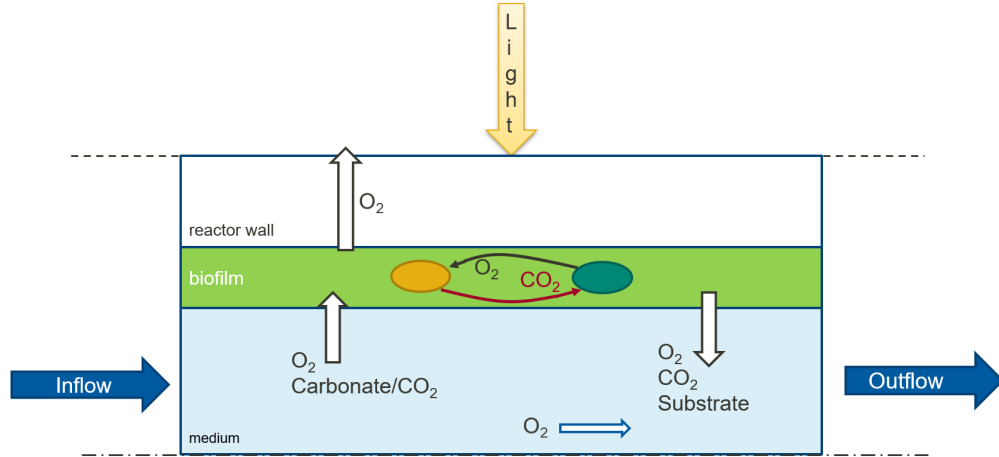
(b) Cultivation unit including the reactor material and the oxygen flux across it into the surrounding environment, in addition to the O_2 accumulation towards the outlet

Figure 5: Scheme of the basic biological processes in the cultivation unit of a Mixed Species Biofilm Capillary Reactor included in the model. Dark green: Phototrophs; Orange: Heterotrophs. White arrows: diffusion mechanisms; Blue arrows: medium flow; Red arrow: CO_2 production and consumption; Black arrow: O_2 production and consumption

3.3 Parameters

Parameters used in the Mixed Species Capillary Biofilm Reactor Model are summarized in Table 1. BDW refers to the Biomass Dry Weight.

Table 1: Parameters included in the Mixed Species Capillary Biofilm Reactor Model

Parameter	Value	Unit	Description	Reference
r_i	1.5	mm	capillary inner radius	This study
d_w	1	mm	reactor wall thickness	This study
d_{bfm}	150	μm	biofilm thickness	David et al. 2015
L	20	cm	capillary length	This study
v_0	52	μL/min	medium flow rate	This study
D_C	$1.18 \cdot 10^{-9}$	m^2/s	diffusion coefficient	Ebrahimi et al. 2003
D_{O_2}	$2.1 \cdot 10^{-9}$	m^2/s	diffusion coefficient	Horn & Hempel 1997
D_S	$0.5 \cdot 10^{-9}$	m^2/s	diffusion coefficient	Horn & Hempel 1997
$P_{O_2,sil}$	500	barrer	permeability of O_2 through silicone	Seader 2011
c_{0,O_2}	254	μmol/m^3	oxygen inlet concentration	This study
$c_{0,C}$	1.791	mol/m^3	carbon inlet concentration	This study
Y_H	0.33	$\frac{\text{gBDW}}{\text{gSubstrate}}$	heterotrophic biomass yield	Heuschkel unpublished
$K_{O_2,het}$	0.0156	mol/m^3	Monod coefficient	Horn & Hempel 1997
$K_{S,het}$	0.125	mol/m^3	Monod coefficient	Horn & Hempel 1997
$K_{C,pho}$	$9.2 \cdot 10^{-4}$	mol/m^3	Monod coefficient	Nguyen & Rittman 2016
K_I	0.1	μmol/m^2	Monod coefficient	Estimated
I_0	50	μmol/m^2	incident light intensity	This study
ke	12	mm^{-1}	light attenuation coefficient	David et al. 2015
f_D	0.5	-	diffusion correction factor	Bryers et al. 1998
f_{dec}	0.2	-	decay fraction	Estimated

3.4 Geometry, Materials and Mesh of the Capillary in COM-SOL

3.4.1 Geometry of the Capillary

For computational reasons, systems can be simplified, as long as no conditions that could affect the results are omitted. The geometry was created as 2D-axisymmetric. The reactor material geometry was not included since mass transport mechanisms across this layer were reduced to a flux at the outer boundary of the biofilm. This abstraction is represented in Fig. 6.

(a) Capillary with two vertical planes

(b) Capillary cut along planes

(c) Front view of the cut capillary
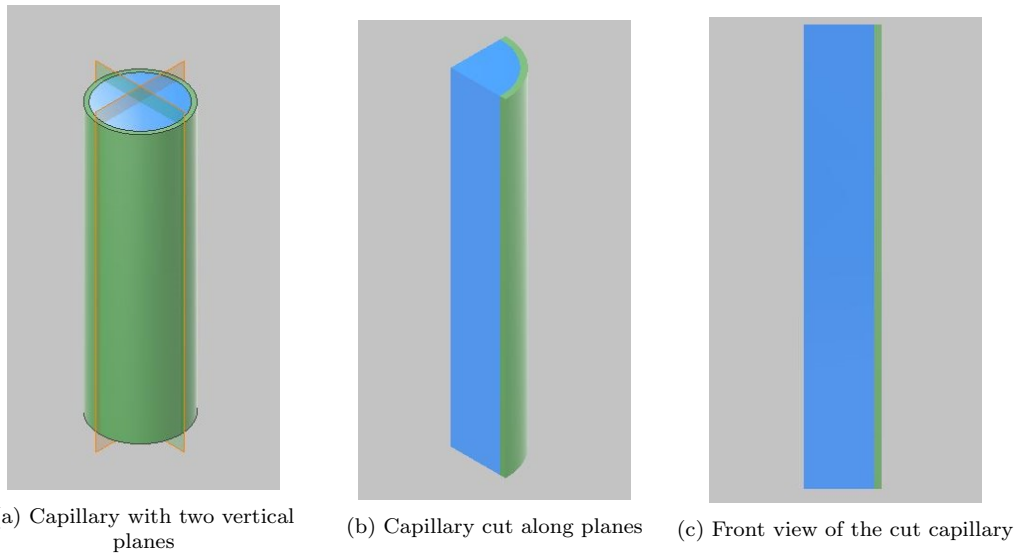
Figure 6: Geometry abstraction of a capillary with medium and biofilm (capillary material layer omitted). Blue: medium; green: biofilm

3.4.2 Materials

Both medium and biofilm were defined as water. Despite the small amount of salt solutions and the few inorganic compounds, the medium is still mostly water, therefore, properties such as viscosity, diffusivity and density are assumed not to change. Hence, no adjustments had to be made when defining it as water.

Due to the fact that the biofilm has more of a gel-like consistency, diffusion in it is slower than in water. Therefore, a correction factor for the diffusion coefficients of components in the biofilm was introduced. As stated in Bryers et al. 1998 [24], diffusion mechanisms in highly hydrated biofilms are 20-50% less than values for pure water. The sensitivity of the model to this factor was tested and its value chosen in section 4.2.1.

3.4.3 Mesh

COMSOL is a simulation software based on advanced numerical methods. Problems concerning laws of physics can usually be expressed through partial differential equations (PDEs). However, in the majority of cases, having complex problems and geometries, these PDEs cannot be solved with analytical methods. Using discretization methods, they can be approximated with numerical model equations. The finite element method is one approach to compute such approximations. The meshing of a model divides it into smaller elements, over which these numerical equations can be solved [25].

The inlet of the capillary is where the first nutrients are taken up by the biofilm from the medium. The boundary between these two components and the biofilm itself is where most processes happen. Since the smaller the elements the more accurate the results, the mesh was chosen to be fine at the inlet as well as at the boundary between the medium and the biofilm (as seen in Fig. 7). However, a fine mesh means a high computational complexity, therefore the elements get bigger towards the center and with the length of the capillary where results can be less accurate. Quadrilateral elements were chosen for this geometry.
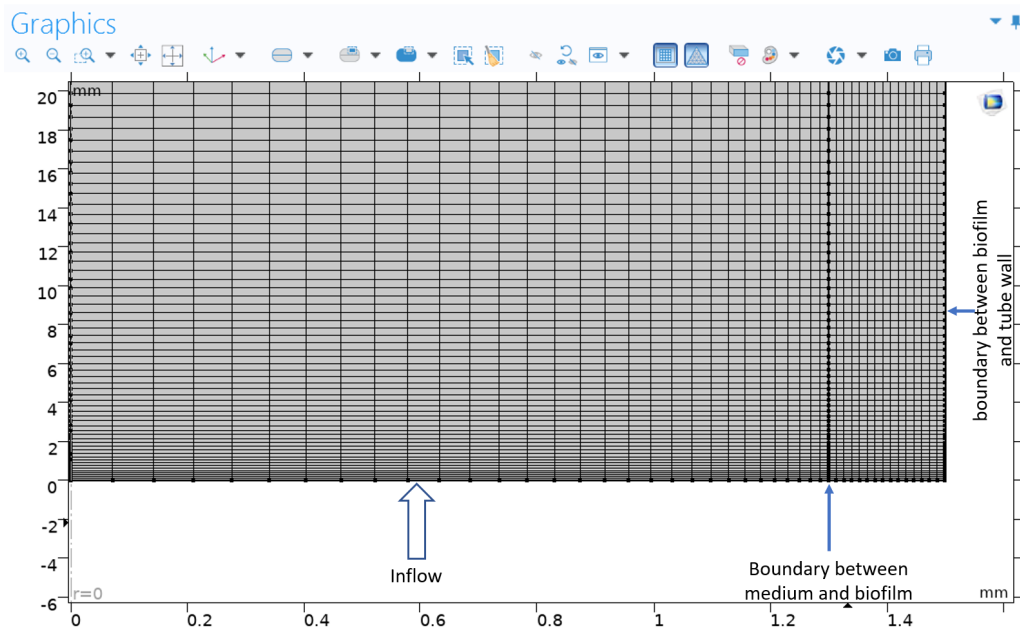
Figure 7: Meshing of the Mixed Species Capillary Biofilm Reactor Model Geometry. Closeup of the bottom right corner: inlet of the capillary and wall between the medium and the biofilm

3.5   Laminar Flow

Having no convection in the biofilm, the laminar flow node was only applied to the medium component. The fluid, here water, was assumed to be incompressible and the flow fully developed. Physical properties, such as dynamic viscosity and density, were taken from the material. The interface between the medium and the biofilm was defined as a no slip wall, where the velocity u is zero.

COMSOL solves the Navier-Stokes equations:

$$\rho(u \cdot \nabla)u = \nabla \cdot [-pI + \mu(\nabla u + (\nabla u)^T)] + F \tag{3}$$

where u is the fluid velocity, p is the fluid pressure, ρ is the fluid density and μ is the fluid dynamic viscosity. The nabla-operator ∇ can be interpreted as a description of the movement of the flow in different directions [26]. The first term $\rho(u \cdot \nabla)u$ corresponds to the inertial forces, the second term $-\nabla pI$ corresponds to the pressure forces, F corresponds to the external forces and the rest to viscous forces.

The equations are always solved with the continuity equation, which represents the conservation of mass:

$$\frac{\partial \rho}{\partial t} + \nabla \cdot (\rho u) = 0 \tag{4}$$

By solving these equations for the particular boundary conditions mentioned above, COMSOL predicts the velocity of the fluid and its pressure in the selected geometry.

3.6   Mass Transfer

3.6.1   Diffusion in the Reactor

The diffusion caused by concentration gradients is described using Fick's Laws [27]:

$$J_i = -D_i \nabla c_i \tag{5}$$

where for the species i, J is the diffusion flux, D the diffusion coefficient and c the concentration. Given the accurate diffusion coefficients, COMSOL solves the equations for the species concentrations.

In the bulk liquid, concentration gradients mean that there is a non uniform concentration distribution of species. Mass transfer caused by diffusion tries to balance this uneven distribution. This mechanism in an immobile fluid is due to the movement

of molecules caused by their thermal energy [27]. When there is bulk liquid motion, it will also contribute to the flux of species. Thus, the fluid velocity was added as convection in the model, to include both the diffusive and the convective flux. The term "convection" refers to the mass transfer due to the velocity of all molecules. The diffusion coefficients for species (oxygen, carbonate and substrate) are provided in Table 1.

As the biofilm is immobile, diffusion in it is only caused by concentration gradients. The same diffusion coefficients that were used for the medium were multiplied by the correction factor f_D to describe the mechanisms taking place in the biofilm (see Fig. 8).
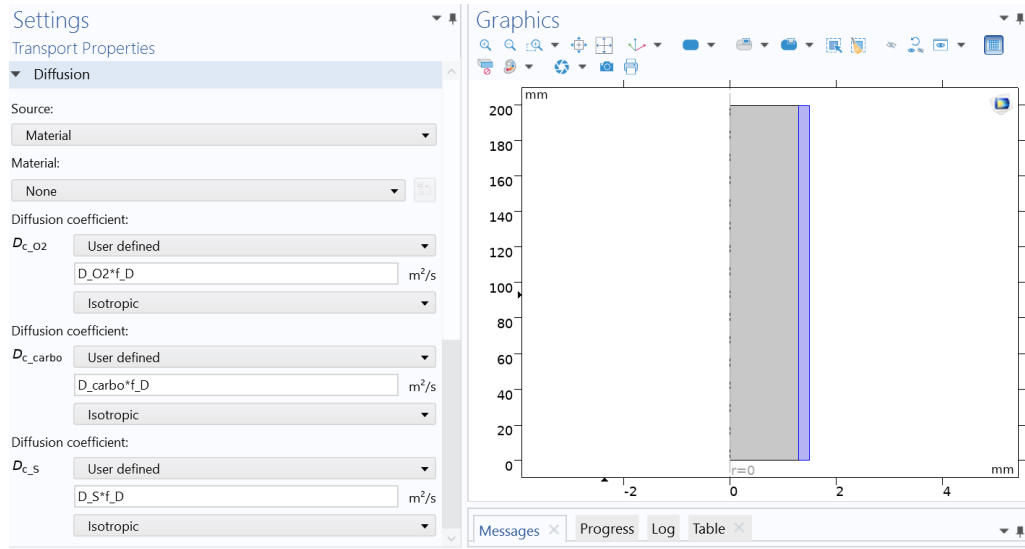
Figure 8: Implementation of the diffusion of oxygen, carbonate and substrate in the biofilm into COMSOL in the Mixed Species Capillary Biofilm Reactor Model. D_i: diffusion coefficients; f_D diffusion correction factor

3.6.2 Oxygen Permeability of the Reactor Material

The flux of oxygen across the outer boundary into the surrounding environment is described as:

$$-n \cdot J_{O_2} = J_{0,O_2} \tag{6}$$

where n is the outward pointing normal of the boundary, J_{O_2} is the oxygen flux and J_{0,O_2} is the prescribed flux specified through the following function:

$$J_{0,O_2} = \frac{P_{O_2,sil}}{d_w} \cdot (c_{0,O_2} - c_{O_2}) \cdot R \cdot T \tag{7}$$

where $P_{O_2,sil}$ is the permeability of the reactor material (here silicone) for oxygen, d_w is the thickness of the reactor material, c_{0,O_2} is the initial oxygen concentration in the reactor material, c_{O_2} is the oxygen concentration in the reactor and R and T are the universal gas constant and the temperature respectively.

Permeability coefficients are often found in literature in the unit "barrer". To convert this unit to SI units, a conversion factor is needed [28]:

$$1\text{barrer} \cdot 3.348 \cdot 10^{-19} = 1 \frac{\text{kmol} \cdot \text{m}}{\text{m}^2 \cdot \text{s} \cdot \text{Pa}} \tag{8}$$

3.7 Cell Growth and Inactivation

The growth rate r_i of a microorganism is expressed through its maximum growth rate $\mu_{\text{max,i}}$, multiplied by the limiting terms f_j and the biomass concentration $c_{X,i}$ [11]:

$$r_i = \mu_{max,i} \cdot c_{X,i} \prod_j f_j \tag{9}$$

Limiting terms were expressed through Monod-type kinetics. They are expressions used to describe bacterial growth and limiting substrates. The Monod model describing the limiting effect of a substrate S on the specific growth rate μ is as follows:

$$\mu = \mu_{max} \cdot \frac{c_S}{k_S + c_S} \tag{10}$$

Where μ_{max} is the maximum specific growth rate, c_S the substrate concentration and k_S the substrate half saturation constant (c_S at half μ_{max}) [29].

In COMSOL the temporal change in cell concentration $c_{X,i}$ was expressed through a Stabilized Convection-Diffusion Equation:

$$\frac{\partial c_{X,i}}{\partial t} = r_{X,i} \tag{11}$$

where $r_{X,i}$ is the growth rate of the microorganism i. The diffusion was set to a minimum (almost zero). By applying this to all heterotrophic, phototrophic and inert cells, the variable density of the biofilm was defined.

3.7.1 Heterotrophic Growth

In this work, heterotrophic organisms are assumed to grow under aerobic conditions, in presence of the O_2 provided through the medium flow and produced by the phototrophs. They consume substrate S as carbon source, which is provided by inert

cells that degrade into organic compounds. The limiting effect of the availability of these substances on cell growth was expressed through Monod kinetics as described earlier. The final equation for the heterotrophic growth rate implemented in the model is:

$$r_{het} = \mu_{max,het} \cdot \frac{c_S}{c_S + k_{S,het}} \cdot \frac{c_{O_2}}{c_{O_2} + k_{O_2,het}} \cdot c_{X,het} \tag{12}$$

3.7.2   Phototrophic Growth

Just like for the heterotrophic growth, the Monod model was applied for the phototrophic microorganisms. Phototrophs do not need oxygen, however their growth is limited by carbonate availability since it serves as carbon source. It is provided through sodium hydrogen carbonate ($NaHCO_3$) in the medium.

Light is the energy source and is a growth limiting factor as well. To take into consideration changes in the intensity, light attenuation through the biofilm was modeled using the Lambert-Beer law [11]:

$$I(r) = I_0 \cdot e^{-ke \cdot (r_i - r)} \tag{13}$$

where I is the light intensity at the coordinate (r,0), r_i is the inner radius of the capillary, I_0 is the incident light intensity and ke the light attenuation coefficient.

Since the oxygen levels in the reactor have an important effect on the phototrophic growth, inhibition through O_2 concentrations was also taken into consideration. Both competitive and non-competitive inhibition types were tested and their effect on the growth rate change observed. Fig. 9 shows that for competitive inhibition, there is no change in the growth rate over the length of the capillary. Whereas, non-competitive inhibition shows a decrease in the rate over the length and time. Comparing the effects of these two growth inhibition types with the experimental observations, the inhibition due to oxygen toxification in the reactor was chosen to be described according to the non-competitive model. Here the inhibition of enzyme functions are generalized for the reaction. This approach models a non-competitive inhibition, where the reaction will never reach its normal maximum rate no matter how much substrate is available, since the reaction pathway is blocked by the inhibitors [13]. This growth limitation was mathematically described through a hill function [30]:

$$f = \frac{K_i}{K_i + c_i} \tag{14}$$

where K_i is a half saturation coefficient of the species i and c_i is its concentration. The final equation implemented in the model for the phototrophic growth rate is:

$$r_{pho} = \mu_{max,pho} \cdot \frac{c_C}{c_C + k_{C,pho}} \cdot \frac{I}{I + k_I} \cdot \frac{K_{O_2,pho}}{K_{O_2,pho} + c_{O_2}} \cdot c_{X,pho} \tag{15}$$

(a) Competitive phototrophic growth inhibition by O_2

(b) Non-competitive phototrophic growth inhibition by O_2
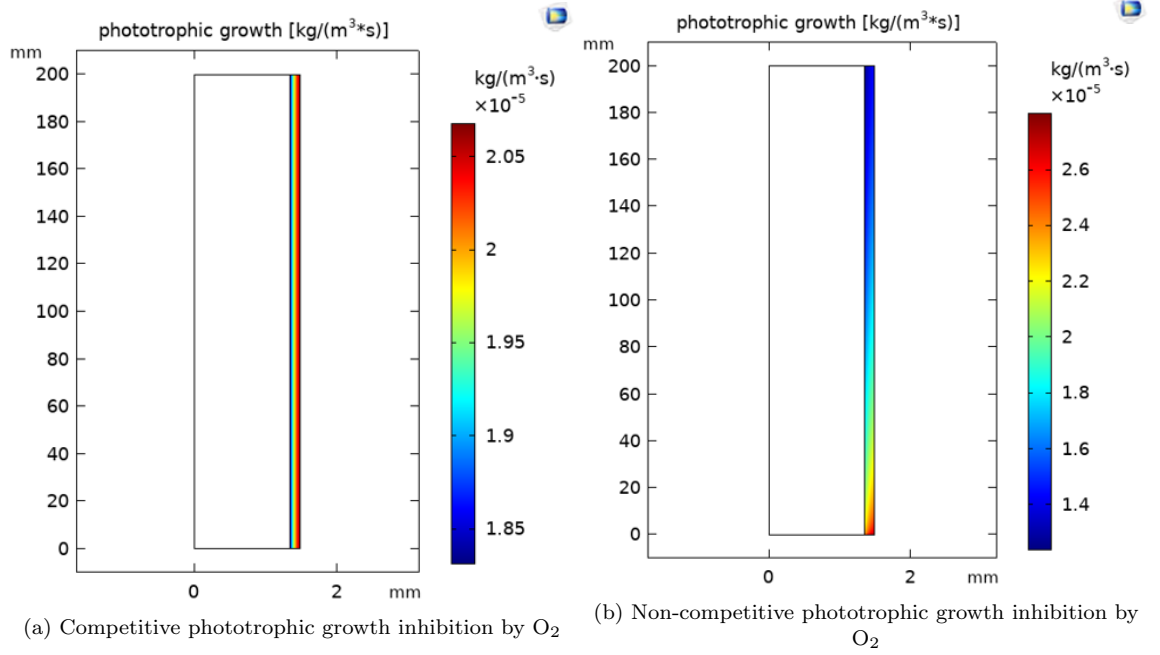
Figure 9: Phototrophic growth rate under competitive and non-competitive growth inhibition by O_2 in COMSOL. White (from 0 to 1.3mm on the horizontal axis and from 0 to 200mm on the vertical axis): medium; Colored: biofilm

3.7.3 Biomass Inactivation

The inactivation of each microorganism $r_{i,ine}$ was expressed through an estimated expression:

$$r_{i,ine} = \frac{\mu_{max,i}}{20} \cdot c_{X,i} \tag{16}$$

where for each growing cell, $\frac{1}{20}$th dies. Both inactive cells and substrate (degraded cells) exist simultaneously in the system, therefore the decay fraction f_{dec} was introduced. Thus, the total amount of inactive cells in the system is described as follows:

$$r_{X,ine} = f_{dec} \cdot (r_{het,ine} + r_{pho,ine}) \tag{17}$$

3.8 Reactions in the Biofilm

Given the appropriate reaction rate r_i that describes the mechanism in the system, COMSOL calculates the concentration c_i of the species i and its changes over the time t:

$$\frac{\partial c_i}{\partial t} \cdot \nabla \cdot J_i + u \cdot \nabla c_i = r_i \tag{18}$$

where u is the velocity, which is 0 in the biofilm and at its boundary to the medium, and J_i is the diffusion flux of the species i.

In this section decay of phototrophic and heterotrophic cells (substrate production) and their consumption is described in addition to the reactions taking place in the reactor concerning oxygen and carbonate. All reaction rates are summarized in Table 2 and Fig. 10 is a reaction scheme with all the included reactions.

3.8.1 Substrate Consumption and Production

Inactive microorganisms are described as inert cells. They slowly degrade producing substrate, which is consumed by the heterotrophic microorganisms. It is assumed that all cells degrade into the same substrate, at the same rate [11]. Therefore, the substrate reaction rate r_S is constituted of two terms, (1) describing the consumption by heterotrophic organisms and (2) describing the production through the decay of inert cells:

$$r_S = \underbrace{S_{S,X,het} \cdot \frac{r_{het}}{M_{S,COD}}}_{1} + \underbrace{\frac{1 - f_{dec}}{M_{S,COD}} \cdot (r_{het,ine} + r_{pho,ine})}_{2} \tag{19}$$

where $M_{S,COD}$ is the molar weight of substrate (expressed through the COD) added for unit conversion, r_{het} the heterotrophic growth rate, f_{dec} the decay fraction of both species and $r_{het/pho,ine}$ the death rate of heterotrophic and phototrophic cells respectively. $S_{S,X,het}$ is a stoichiometric factor taken from the PHOBIA model, this is further explained in section 3.9.

3.8.2 Oxygen Consumption and Production

The oxygen reaction rate r_{O_2} is composed of two terms, (1) the consumption by the heterotrophic cells and (2) the production by the phototrophic cells:

$$r_{O_2} = \underbrace{S_{O_2,X,het} \cdot \frac{r_{het}}{M_{O_2}}}_{1} + \underbrace{S_{O_2,X,pho} \cdot \frac{r_{pho}}{M_{O_2}}}_{2} \tag{20}$$

where M_{O_2} is the molar weight of oxygen, $r_{pho/het}$ are the phototrophic and heterotrophic growth rates respectively and $S_{O_2,X,het}$ and $S_{O_2,X,pho}$ the stoichiometric coefficients taken from the PHOBIA model (section 3.9).

3.8.3 Carbonate Consumption and Production

In analogy to substrate and oxygen, the carbonate reaction rate r_C is also composed of two terms, (1) describing the carbonate consumption by phototrophs and (2) the production by heterotrophs in form of CO_2:

$$r_C = \underbrace{S_{C,X,pho} \cdot \frac{r_{pho}}{M_C}}_{1} + \underbrace{S_{C,X,het} \cdot \frac{r_{het}}{M_C}}_{2} \tag{21}$$

where M_C is the molar weight, $r_{pho/het}$ are the phototrophic and heterotrophic growth rates respectively and $S_{C,X,het}$ and $S_{C,X,pho}$ the stoichiometric coefficients taken from the PHOBIA model (section 3.9).
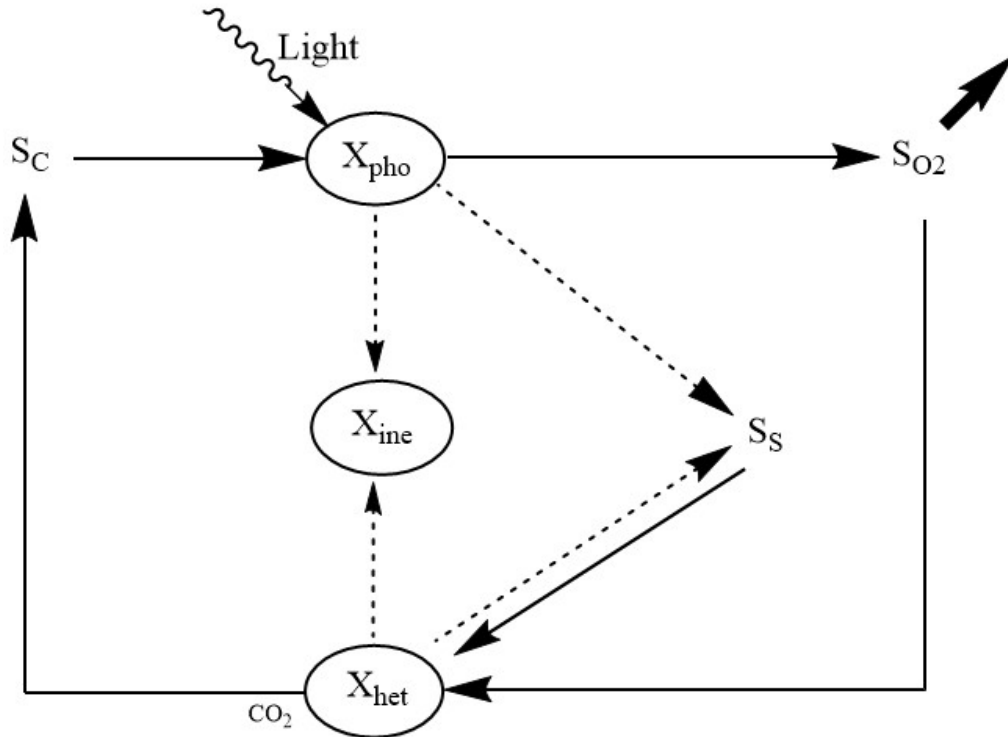
Figure 10: Reaction Scheme: conversion processes and interactions between microbial groups in the mixed species biofilm. Full lines: Growth-related processes; broken lines: biomass inactivation and decay-related processes

24

Table 2: Rate expressions of the biological processes in the model

| Rate	Expression	Description
r_{het}	$\mu_{max,het} \cdot \frac{c_S}{c_S+k_{S,het}} \cdot \frac{c_{O_2}}{c_{O_2}+k_{O_2,het}} \cdot c_{X,het}$	Heterotrophic growth rate
r_{pho}	$\mu_{max,pho} \cdot \frac{c_C}{c_C+k_{C,pho}} \cdot \frac{I}{I+k_I} \cdot \frac{K_{O_2,pho}}{K_{O_2,pho}+c_{O_2}} \cdot c_{X,pho}$	Phototrophic growth rate
$r_{het,ine}$	$\mu_{max,het} \cdot \frac{c_{X,het}}{20}$	Heterotrophic inactivation rate
$r_{pho,ine}$	$\mu_{max,pho} \cdot \frac{c_{X,pho}}{20}$	Phototrophic inactivation rate
$r_{X,ine}$	$f_{dec} \cdot (r_{het,ine} + r_{pho,ine})$	Biomass inactivation
r_S	$S_{S,X,het} \cdot \frac{r_{het}}{M_{S,COD}} + \frac{1-f_{dec}}{M_{S,COD}} \cdot (r_{het,ine} + r_{pho,ine})$	Substrate reaction rate
r_{O_2}	$S_{O_2,X,pho} \cdot \frac{r_{pho}}{M_{O_2}} + S_{O_2,X,het} \cdot \frac{r_{het}}{M_{O_2}}$	Oxygen reaction rate
r_C	$S_{C,X,pho} \cdot \frac{r_{pho}}{M_C} + S_{C,X,het} \cdot \frac{r_{het}}{M_C}$	Carbonate reaction rate

3.9   Model Stoichiometry

The stoichiometry from the PHOBIA model was used as basis for this work. These stoichiometric factors were mathematically fitted to fulfill the mass balance. In the original work by Wolf et al. [11] rates concerning internal polyglucose and EPS production were included, these are zero in this work since the associated processes were not taken into account. The factors for the oxygen reaction rate were oxygen based and related to the oxygen production rate by the phototrophic organisms. For reasons of consistency and data availability, these factors were adapted to be biomass based and related to the maximum phototrophic growth rate. For the biological processes modeled, the appropriate stoichiometric factors are summarized in Table 3.

In the field of wastewater treatment, it is very common to express organic constituents as amounts of chemical oxygen demand (COD) [31]. Therefore, to ensure that results from this work are comparable with previous studies, organic compounds are expressed through their COD. "The COD is defined as the amount of oxygen equivalents consumed in the chemical oxidation of organic matter by strong oxidants." (Z. Hu & D. Grasso, 2005, page 1) [32].

Table 3: Stoichiometry table of the biological processes included in the Mixed Species Capillary Biofilm Reactor Model

Process	Particulates			Solubles		
	X_{Pho}	X_{Het}	X_{Ine}	S_C	S_{O_2}	S_S
	$\mathrm{kg_{COD}m^{-3}}$	$\mathrm{kg_{COD}m^{-3}}$	$\mathrm{kg_{COD}m^{-3}}$	$\mathrm{kmolm^{-3}}$	$\mathrm{kmolm^{-3}}$	$\mathrm{kg_{COD}m^{-3}}$
Phototrophic growth on HCO$_3$	1			$-\frac{1.0025}{32}$	$\frac{32}{1.3409}$	
Phototrophic inactivation	-1		f_{dec}			$1 - f_{dec}$
Heterotrophic growth (aerob)		1		$\frac{1}{32 \cdot Y_H} - 0.02976$	$-\frac{1}{32 \cdot Y_H} + 0.03125$	$-\frac{1}{Y_H}$
Heterotrophic inactivation		-1	f_{dec}			$1 - f_{dec}$

3.10 Initial Values and Model Kinetics Determination

In order to make sure that the model describes the biological system as accurately as possible, initial conditions and kinetics were determined and implemented. Initial cell concentrations in the reactor at the time of inoculation were calculated, oxygen and carbonate concentrations in the medium were measured and the growth rates of microorganisms in biofilms were determined.

3.10.1 Oxygen and Carbonate Measurements

The oxygen concentration c_{0,O_2} in the medium was measured with an optical sensor from PyroScience GmbH (Aachen Germany) for measurements in the liquid. The sensor was calibrated with air saturated water. It emits red excitation light and detects the luminescence caused by the collision of oxygen molecules and this excitation light [33]. Since the amount of dissolved oxygen in the liquid is temperature dependent, the ambient temperature was measured simultaneously with a Pt100 temperature sensor. For measurements in the liquid, the tip of the sensor was submerged in the medium accumulated at the bottom of the bubble trap. For gas-phase measurements, the tip was only in contact with the gas that accumulated in the bubble trap and the sensor was calibrated with ambient air. In addition to the initial O_2 concentration measurement in the liquid, all other measurements during the experiments, were performed following the method of the gas-phase concentration determination.

Even though a specified amount of $NaHCO_3$ is added to the medium, the carbonate concentration at the inlet of the cultivation unit $c_{0,C}$ was measured. It is not yet clear if carbon dioxide dissolves into the medium due to the alkaline pH caused by the bacteria in the reactor [34], or if, following Le Chatelier's Principle, carbonate diffuses out of the medium due to its high concentration [35]. To overcome this uncertainty, $c_{0,C}$ was chosen to be measured. For that purpose, 8 mL samples were taken from the inlet of the cultivation unit. These samples were then prepared for the carbonate concentration determination by adding 2 mL of 10M sodium hydroxide (NaOH) and 30 mL deionized water. Due to the contact with NaOH, the carbonate stays in solution and can be detected and quantified.

3.10.2 Initial Cell Concentrations

The initial cell concentration $c_{0,X,pho}$ and $c_{0,X,het}$ for *Synechocystis* and *P. taiwanensis* respectively were calculated based on cell count data from Martin Schuster's Project Work. In his work the amount of colony forming units (cfu) per volume unit was

determined. This method only takes into consideration viable cells and results at the point of inoculation are comparable with number of cells per volume unit.

For *Synechocystis*, having an initial cell number of $N_{pho} = 23250000 \text{cfu/mL}$ and the weight of a single cell $m_{pho} = 5396\text{fg}$ [36], the initial cell concentration could be determined as follows:

$$c_{0,X,pho} = N_{pho} \cdot m_{pho} \tag{22}$$

$$c_{0,X,pho} = 23250000 \frac{1}{\text{mL}} \cdot 5396\text{fg} \tag{23}$$

$$c_{0,X,pho} = 0.1255\text{g/L} \tag{24}$$

For *P. taiwanensis*, having an initial cell number of $N_{het} = 64430000\text{cfu/mL}$ and the weight of a single cell $m_{het} = 1100\text{fg}$ [37], the initial cell concentration could be determined as follows:

$$c_{0,X,het} = N_{het} \cdot m_{het} \tag{25}$$

$$c_{0,X,het} = 64430000 \frac{1}{\text{mL}} \cdot 1100\text{fg} \tag{26}$$

$$c_{0,X,het} = 0.0709\text{g/L} \tag{27}$$

3.10.3   Growth Rate Determination

The growth rates for both *Synechocystis* and *P. taiwanensis* were determined using fluorescence measurements from Martin Schuster's Project Work. Samples were taken from a Mixed Species Capillary Biofilm Reactor at different times and the fluorescence of *Synechocystis* and *P. taiwanensis* was detected. *Synechocystis* are autofluorescent when excited, whereas *P. taiwanensis* are marked with a green fluorescent protein (gfp). Assuming exponential growth (Fig. 11) and that the number of active cells is directly linked to the fluorescence of the biomass sample, the cell concentrations could be determined. Maximum growth rates $\mu_{max,i}$, for phototrophic and heterotrophic cells were determined as follows [38]:

$$F_i(t) = F_{0,i} \cdot e^{\mu_{max,i} \cdot t} \tag{28}$$

where $F_i(t)$ is the fluorescence at the time t and $F_{0,i}$ is the initial fluorescence of the sample. Solving for $\mu_{max,i}$:

$$\mu_{max,i} = \frac{1}{t} \cdot \ln \frac{F_i(t)}{F_{0,i}} \tag{29}$$

For *Synechocystis* for instance, the initial fluorescence was $F_{0,Syn} = 111516.67\text{FU}/\text{V}_r$, for $t = 2.96\text{d}$ it was $F_{Syn}(t = 2.96\text{d}) = 698424.80\text{FU}/\text{V}_r$, the maximum growth rate could be calculated as follows:

$$\mu_{max,Syn}(t = 2.96\text{d}) = \frac{1}{2.96\text{d}} \cdot \ln \frac{698424.80\text{FU}/\text{V}_r}{111516.67\text{FU}/\text{V}_r} \tag{30}$$

$$\mu_{max,Syn}(t = 2.96\text{d}) = 0.62\text{d}^{-1} \tag{31}$$

These calculations were repeated using data from 2 reactors to obtain an average value. The maximum growth rate $\mu_{max,het}$ for *P. taiwanensis* was determined following the same method. Results are stated in section 4.2.2.
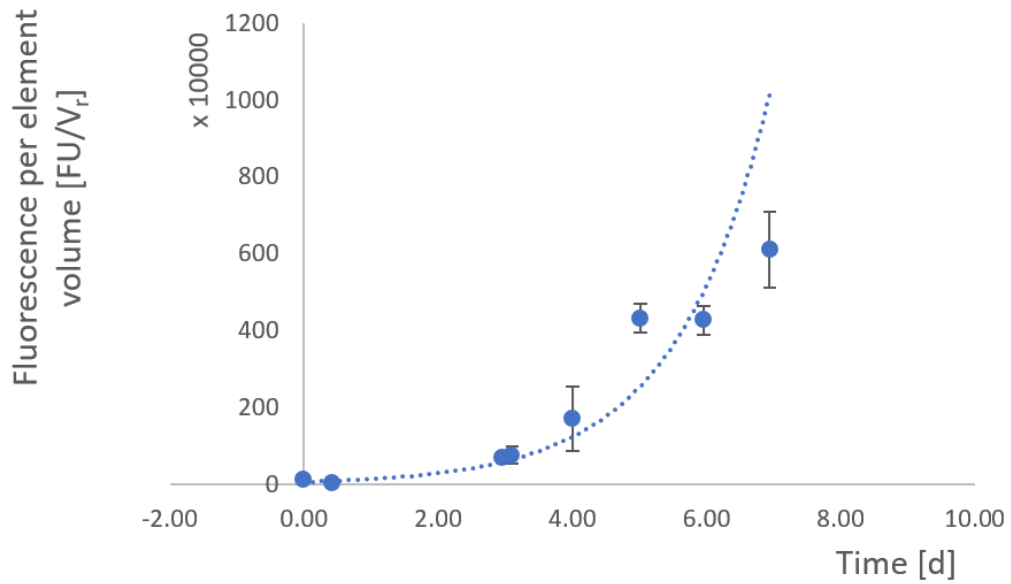
Figure 11: Growth of *Synechocystis* in a capillary reactor, cell numbers detected through their fluorescence. Data from Martin Schuster's Project Work

4 Results

The aim of this model was to provide the opportunity to evaluate different attachment materials focusing on their oxygen permeability, as well as different lengths and their effects on O_2 concentrations and cell growth. To achieve this goal the model had to be adapted to the biological system, this was mainly done by comparison of model and experimental results and by implementing the parameters that were determined through experiments into the model.

4.1 Medium Flow through the Capillary Reactor

For the sake of simplicity, only a single phase flow (without air segments) was considered. The flow rate of the medium through the capillary in the model was set to $v_0 = 52\mu L/min$, as this is the standard flow velocity in the experiments. Different flow rates can be tested and their effect on the biomass formation analyzed, however since the biofilm deformation is not taken into account in this model, the effect of shear forces on biofilm detachment and on nutrient availability was not considered. The velocity plot (Fig. 12) corresponds to the parabolic profile of a fully developed, laminar flow (as expected when calculating the corresponding Reynolds Number $Re = 2.122$). This is due to the movement of adjacent layers through the capillary. Viscous interactions between layers of the medium and the wall of the biofilm are minimized. As can be observed in Fig. 12, the velocity is zero at the immobile wall (boundary between medium and biofilm) and at its maximum in the center of the capillary.
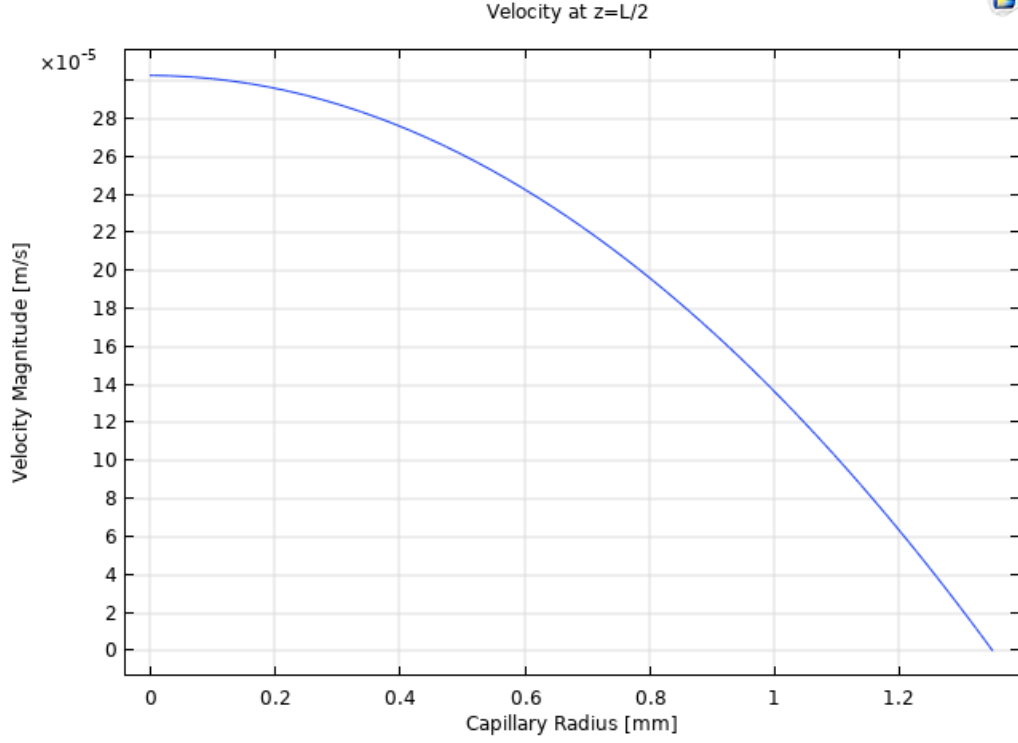
Figure 12: Velocity of the medium flow through the capillary (at z=10cm) in the Mixed Species Capillary Biofilm Reactor Model. 0 on the horizontal axis: center of the capillary; 1.5mm on the horizontal axis: boundary between biofilm and reactor material

The simulation confirmed a laminar flow of the nutritional medium through the cultivation unit capillary.

4.2   Implementation of Determined Parameters

4.2.1   Biofilm Thickness and Diffusion Correction Factor

The model considered a mature biofilm with a constant thickness over time and over the length of the capillary. It was set to the maximum average thickness reached in experiments, which was determined by David et al. to be $d_{bfm} = 150\mu$m. The cell concentration, that is the distribution of the two species and the localisation of the organisms in the three dimensional structure, is variable depending on the growth rates of the microorganisms. The diffusion correction factor f_D was introduced to adjust the diffusion coefficients for water to be suitable for the biofilm. f_D was estimated by Bryers et al. to be between 0.2 and 0.5. The sensitivity of the model to this parameter was tested. An increase by 400% in the correction factor, affects the results for oxygen concentrations by 0.04% and carbonate concentrations by 0.008%. As these effects are negligible, 0.5 was chosen as value for f_D, assuming the slowest diffusion.

4.2.2 Initial Values and Growth Rates

The oxygen and carbonate concentrations in the medium were measured as described in section 3.10.1. The results were as follows:

$$c_{0,O_2} = 0.254 \mu\text{mol/m}^3 \tag{32}$$

$$c_{0,C} = 1.791 \text{mol/m}^3 \tag{33}$$

The initial cell concentrations $c_{0,X,pho}$ and $c_{0,X,het}$ were determined as described in section 3.10.2:

$$c_{0,X,pho} = 0.1255 \text{g/L} \tag{34}$$

$$c_{0,X,het} = 0.0709 \text{g/L} \tag{35}$$

The growth rates μ_{pho} and μ_{het} for *Synechocystis* and *P. taiwanensis* respectively, were determined according to the approach mentioned in section 3.10.3:

$$\mu_{max,pho} = 0.008 \text{h}^{-1} \tag{36}$$

$$\mu_{max,het} = 0.018 \text{h}^{-1} \tag{37}$$

To achieve an accurate description of the modeled system, all parameters that were measured during experiments that describe the initial conditions in the reactor, as well as the calculated kinetics from experimental data that are specific for this reactor, were implemented.

4.3 Inhibition Term Reduces Biofilm Formation in the Model

The implementation of a term that models the growth rate inhibition with increasing oxygen concentration (section 3.7.2) resulted in a biomass distribution that describes the growth behavior of the biological system more accurately. Fig. 13 shows the biomass concentration in the oxygen impermeable reactor model where the phototrophic growth is not inhibited by the oxygen levels. The biofilm is evenly distributed along the capillary wall and the only change in density observed is due to the light attenuation.

Figure 13: Distribution of the biofilm in the Mixed Species Capillary Biofilm Reactor Model (oxygen impermeable) on day 14, without growth inhibition. Left: Capillary inlet; right: capillary outlet. White (from 0 to 1.3mm on the vertical axis and from 0 to 200mm on the horizontal axis): medium; colored: biofilm

Fig. 14 on the other hand shows an uneven biofilm distribution, where the density decreases with the length of the capillary and with that the increasing O_2 concentrations. This effect is usually observed in experiments. Fig. 15 is an image of the capillary from a polystyrene Mixed Species Photo Biofilm Reactor. On the left (capillary inlet) a dense biofilm can be observed, the biofilm formation decreases with the length of the tube. The yellowish color indicates oxygen toxification, this leads to biofilm detachment (parts of the biofilm are flushed out with the medium flow). Detachment was not modeled, therefore in the reactor model the capillary is completely covered in biofilm.
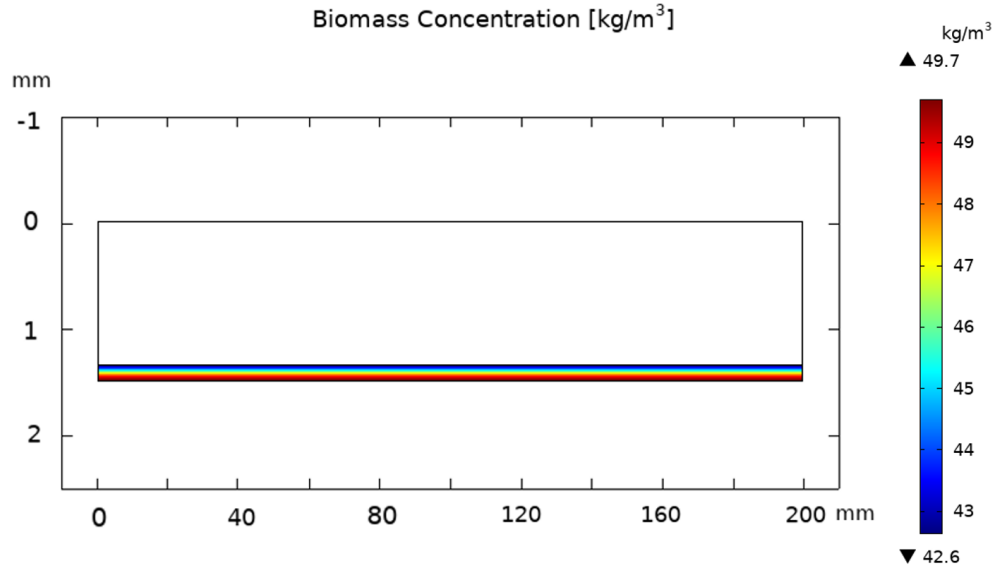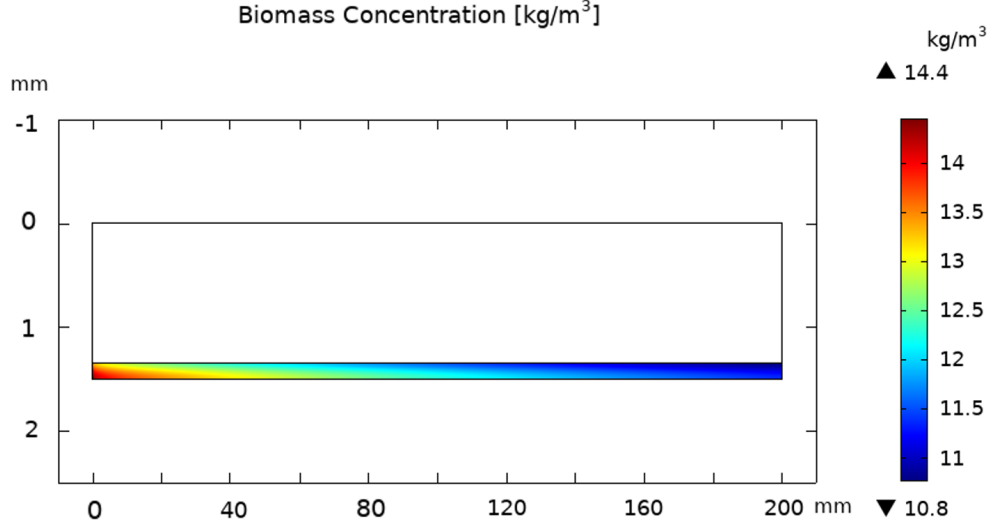
Figure 14: Distribution of the biofilm in the Mixed Species Capillary Biofilm Reactor Model (oxygen impermeable) on day 14, with growth inhibition. Left: Capillary inlet; right: capillary outlet. White (from 0 to 1.3mm on the vertical axis and from 0 to 200mm on the horizontal axis): medium; colored: biofilm
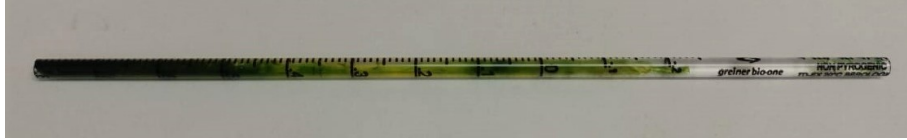
Figure 15: 20 cm capillary (cultivation unit) of 3mm diameter, from a polystyrene photobioreactor on day 14. Left: capillary inlet; right: capillary outlet. Dense dark green biomass at the inlet, yellowish biomass towards the outlet, due to oxygen toxification. Cells cultivated under 50μmol/m^2 light intensity and 52μL/min medium flow velocity

Through the inhibition term the amount of biomass produced in the model was also reduced to a value that is a lot more realistic and comparable with experimental results (11.50 ± 1.97g$_{\mathrm{BDW}}$/L for a polystyrene reactor on day 14). Table 4 summarizes the final average biomass concentrations reached with and without the implementation of this inhibiting term.

Table 4: Final Average Biomass Concentration $c_{X,final}$ in oxygen impermeable Reactor Model With and Without Growth Inhibition Term

Phototrophic Growth Rate	$c_{X,final}$
$r_{pho} = \mu_{max,pho} \cdot \frac{c_C}{c_C+k_{C,pho}} \cdot \frac{I}{I+k_I} \cdot c_{X,pho}$	47.1g$_{\mathrm{BDW}}$/L
$r_{pho,inhib} = \mu_{max,pho} \cdot \frac{c_C}{c_C+k_{C,pho}} \cdot \frac{I}{I+k_I} \cdot \frac{K_{O_2,pho}}{K_{O_2,pho}+c_{O_2}} \cdot c_{X,pho}$	12.4g$_{\mathrm{BDW}}$/L

Including an inhibition term for phototrophic growth due to oxygen toxification was a crucial step towards an accurate description of the growth behavior of cells in the cultivation unit of the Mixed Species Capillary Biofilm Reactor.

4.4 Impact of Oxygen Permeability of the Reactor Material on Oxygen Concentration, Carbonate Consumption and Biofilm Formation

4.4.1 Impact of Oxygen Permeability of the Reactor Material on Oxygen Concentrations

Comparing oxygen concentrations from a model where gas permeability of the material the cultivation unit is made of, is included with those from a gas impermeable reactor model, the concentrations in reactors where O_2 does not diffuse into the surrounding area, are around 5% higher at the beginning and around 1.4% higher at the end of the simulation. The concentrations in Fig. 16 are measured at the same point at the outlet of the capillary (gas permeability/impermeability refers to oxygen only). The oxygen concentrations in the permeable reactor model seems to have a steeper slope than in the oxygen impermeable reactor model. This could be due to the less hampered growth of phototrophs.
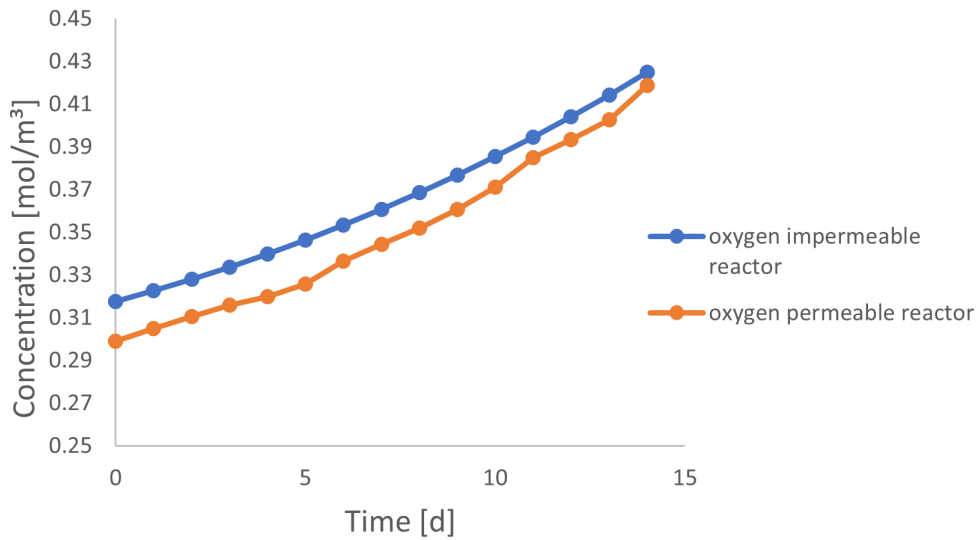
Figure 16: Oxygen concentrations in the Mixed Species Capillary Biofilm Reactor Model with and without oxygen permeability simulating the O_2 flux over the cultivation unit material in the reactor

Fig. 17 shows two path plots on day 14 of the simulation, for oxygen concentrations at 3 different lengths in both the oxygen permeable and the oxygen impermeable reactor. In both graphs the O_2 concentration increases over the length on the capillary, since the oxygen accumulates towards the end of the capillary as observed in experiments through the toxification and growth inhibition of cells. Also, in both graphs the concentration is higher in the biofilm where phototrophs produce oxygen

and lower in the medium, into which it diffuse due to the lower inlet concentration. The difference between the two graphs can be observed towards the outer boundary of the biofilm, where in the left model a flux of O_2 into the surrounding area was introduced. On the left, where the oxygen permeability was implemented, the concentration drops towards the outer boundary due to the mass transport of O_2 into the adjacent environment. In contrary, in the graph on the right, the concentration continues to increase until it reaches the maximum at the outer boundary. Other than observed in Fig. 16, the oxygen has a seemingly higher concentration towards the center of the capillary in the model with O_2 permeability. The reason behind this has yet to be investigated.

Figure 17: O_2 concentrations at different positions in the Mixed Species Capillary Biofilm Reactor Model on day 14. Left: model with oxygen permeability of the reactor cultivation unit material; right: model without oxygen permeability of the reactor cultivation unit material

Results from the O_2 impermeable reactor model were compared to results from experiments conducted with polystyrene as reactor material (because of its low permeability). Both the simulation and the experiments were run with a capillary of the length L=20 cm. Experimental results were obtained from a previous work. Fig. 18 shows these O_2 concentrations over the time. An increase in both data sets can be observed. While the concentration in the experiments continuously increases, the concentration in the model seems to reach a plateau at around $c_{O_2,model} = 0.45$mol/m^3. In reality O_2 concentrations continue as long as phototrophs are active, even though toxification and growth inhibition occurs, cells still produce oxygen near the inlet of the cultivation unit, which accumulates towards the outlet. In the reactor model, the oxygen production seems to reach a maximum which could be linked to the decrease of the phototrophic growth rate over the whole biofilm.

Figure 18: O_2 concentrations in the Mixed Species Capillary Biofilm Reactor Model where oxygen permeability of the cultivation unit material was not included, and O_2 concentrations in the experiment with polystyrene as reactor cultivation unit material. Concentrations are measured at the outlet of the cultivation unit

Experimental data for an experiment run with a silicone reactor of the length L=1m, is obtained from unpublished work by Heuschkel (2019). The O_2 permeability for silicone was taken from Seader 2011 [28] and implemented according to section 3.6.2. This data was compared to model results where the gas permeability was included and the reactor length was set to L=1m. Fig. 19 shows the O_2 concentrations in the model and the experiment over the time. While the experimental results seem to reach a plateau, where the oxygen does not increase significantly, the model results seem to show an exponential, unhampered increase in concentrations. This could be due to too low growth inhibition, since the production of oxygen by heterotrophs should reach a maximum as observed in experiments.
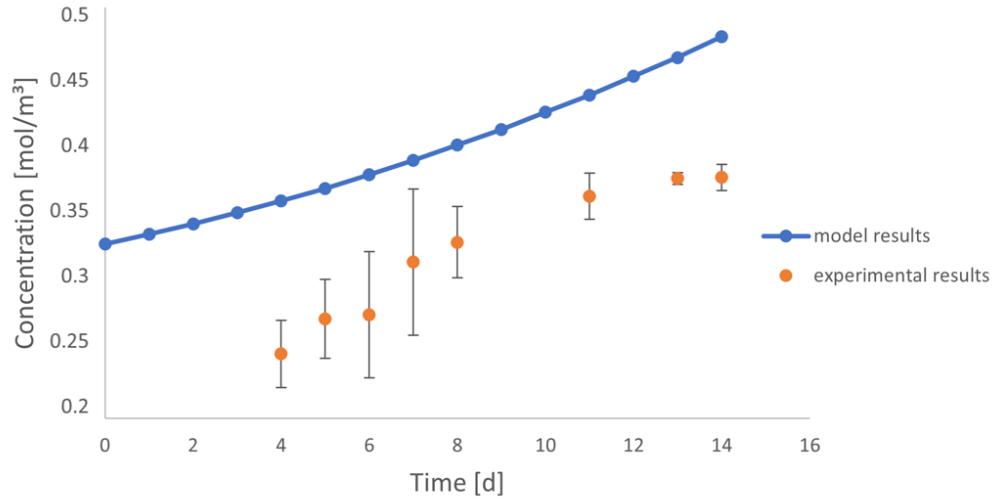
Figure 19: O_2 concentrations in the Mixed Species Capillary Biofilm Reactor Model with included oxygen permeability of the cultivation unit material, and O_2 concentrations in the experiment with silicone as reactor cultivation unit material. Concentrations are measured at the outlet cultivation unit

Even though the overall oxygen concentrations in a model with included reactor material permeability is seemingly lower than those without, the evolution of model results over the time do not match the experimental measurements yet.

4.4.2 Impact of Oxygen Permeability of the Reactor Material on Carbonate Concentrations

The permeability of CO_2 was not included in the model, all changes stated in this section are solely due to the mass transport of O_2 from the reactor into the surrounding area and the effect of that on cell growth (gas permeability/impermeability refers to oxygen only). Fig. 20 shows the carbonate consumption in an oxygen permeable reactor model in comparison with an oxygen impermeable reactor model. In the oxygen permeable reactor the carbonate consumption is around two times higher than in the impermeable reactor model, as the phototrophic cells are more active due to lower O_2 toxification. Fig. 21 shows path plots of the carbonate concentration at different positions in the oxygen impermeable and the oxygen permeable reactor models on day 14. The concentration is the highest at the center of the capillary, it diffuses into the biofilm where it is consumed by the phototrophic microorganisms, the higher carbonate consumption can be observed as well.
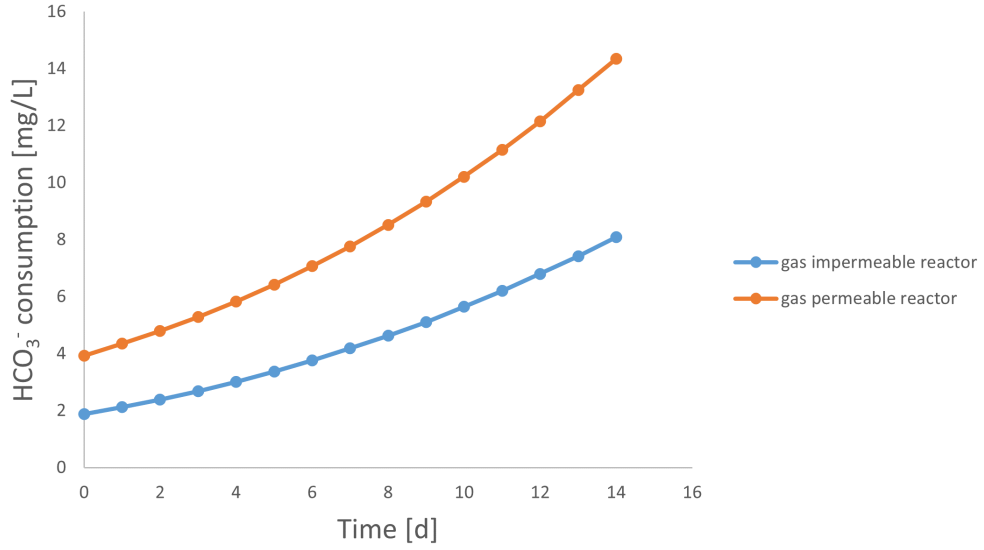
Figure 20: Carbonate consumption in the Mixed Species Capillary Biofilm Reactor Models with and without oxygen permeability with and without oxygen permeability simulating the O_2 flux over the cultivation unit material in the reactor
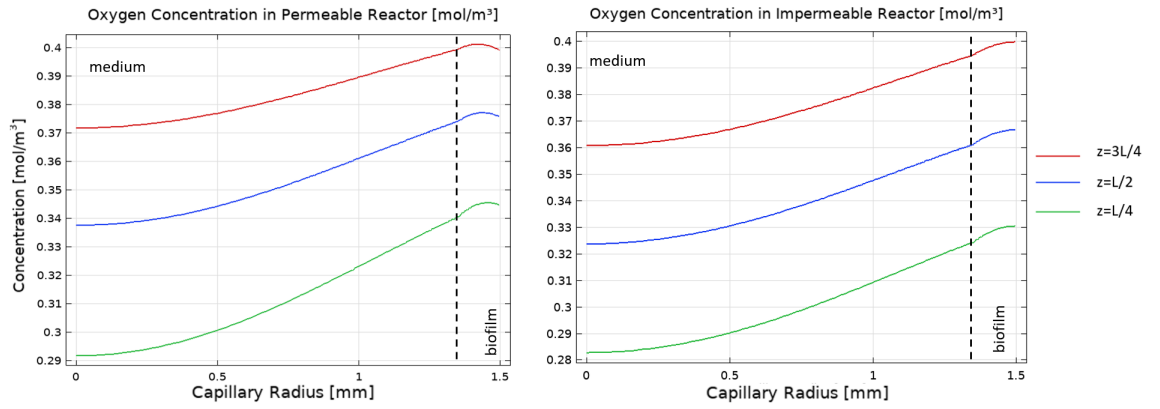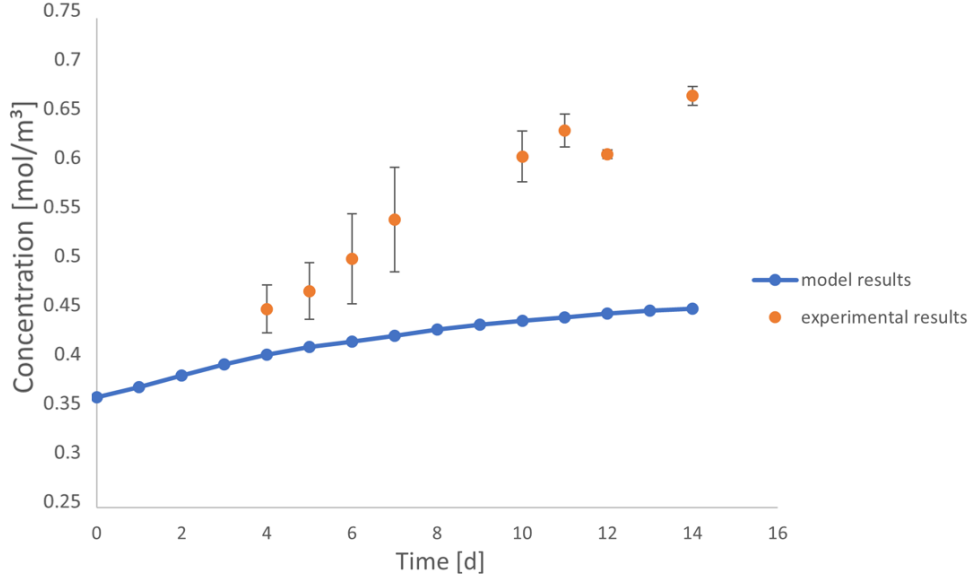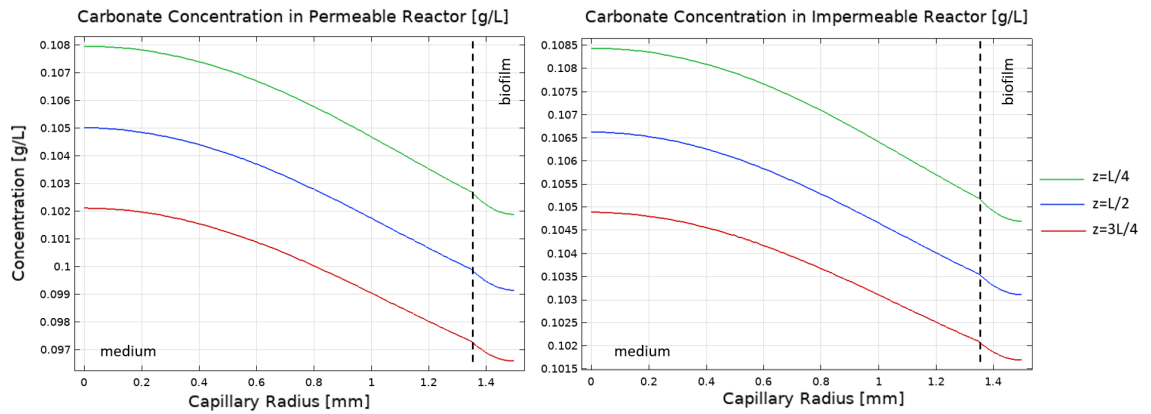

Figure 21: Carbonate concentration at different positions in the Mixed Species Capillary Biofilm Reactor Models on day 14. Left: model with oxygen permeability of the reactor cultivation unit material; right: model without oxygen permeability of the reactor cultivation unit material

An accurate assessment of the effects of the reactor material permeability on the carbonate consumption is difficult at this stage of the model due to the lack of including the CO_2 permeability. However, results deliver that lower oxygen concentrations in the cultivation unit lead to a higher carbonate consumption.

4.4.3 Impact of Oxygen Permeability of the Reactor Material on Biofilm Formation

Fig. 22 shows the biomass distribution in the biofilm in the oxygen permeable reactor model. Comparing these results to the results in Fig. 14, a similar distribution of the biomass can be observed. Towards the outlet of the capillary the concentration decreases. While, for the oxygen impermeable reactor model, the cell growth reaches its minimum at a capillary length of around 130mm, it is only attained at around 180mm for the oxygen permeable reactor model. The overall concentration reached in the permeable reactor model is around 5g/L higher than in the impermeable reactor model.
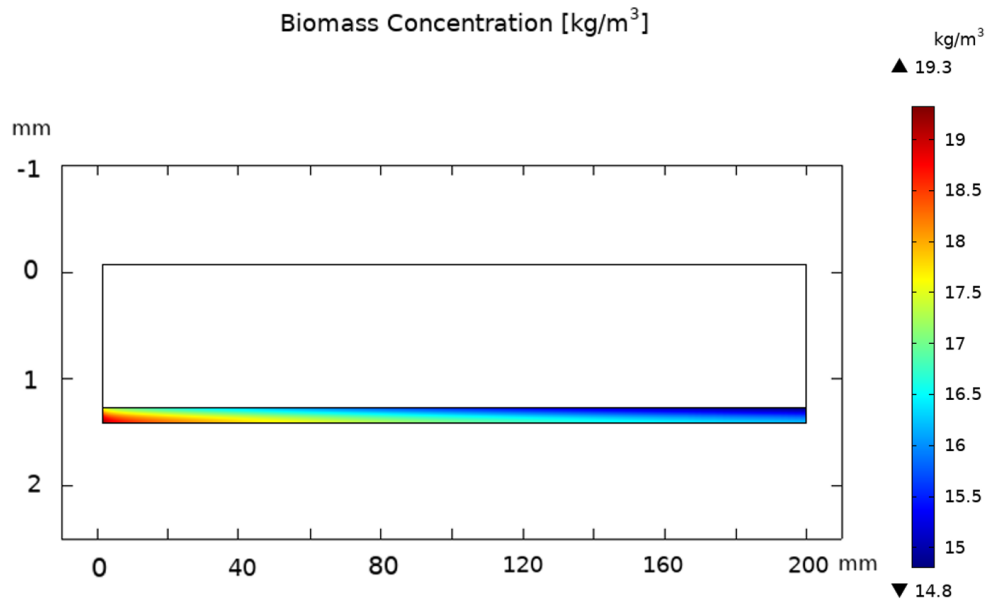
Figure 22: Distribution of the biofilm in the Mixed Species Capillary Biofilm Reactor Model where oxygen permeability of the cultivation unit material on day 14. Left: Capillary inlet, right: capillary outlet. White (from 0 to 1.3mm on the vertical axis and from 0 to 200mm on the horizontal axis): medium, colored: biofilm

The average biomass concentrations from both the oxygen permeable and impermeable reactor models are displayed in the bar graph in Fig. 23, together with the experimental results from polystyrene and silicone reactors. Experimental data for the silicone reactor was obtained from previous work by I. Heuschkel. For the oxygen impermeable model, the biomass concentration fits the experimental results from the polystyrene reactor. The biomass concentration in the oxygen permeable model is around 1.7 times lower than the results from the silicone reactor. The O_2 permeability facilitates biofilm formation.

40
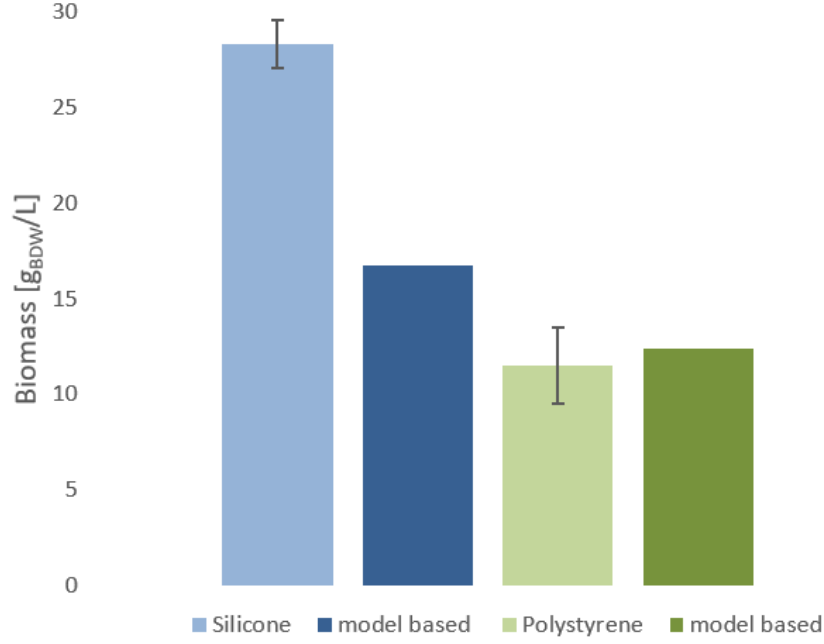
Figure 23: Biomass concentration for different reactor materials and the corresponding reactor model results

An oxygen permeable reactor material enables the cultivation of high cell density biofilms.

4.5 Impact of Reactor Scale-Up on Oxygen Concentrations and Biofilm Formation

The determination of the appropriate reactor material, that enables enough gas permeability to reduce the oxygen toxification and growth inhibition, is crucial for the next step: reactor scale-up. For the oxygen permeable model created in this work, two different reactor lengths were tested; L=1m and L=20cm. Fig. 24 shows the oxygen concentrations at the outlet of the reactor for these two capillary lengths. Concentrations in the 1m tube are maximum 1.15 times higher than those in the 20cm tube. Fig. 25 shows the biomass concentration in a 1m oxygen permeable reactor model. The distribution is similar to that in a 20cm reactor, with high density at the inlet (here bottom) and lower density at the outlet. The biomass production reaches its minimum at almost 50cm and cells continue to grow with a slower rate.
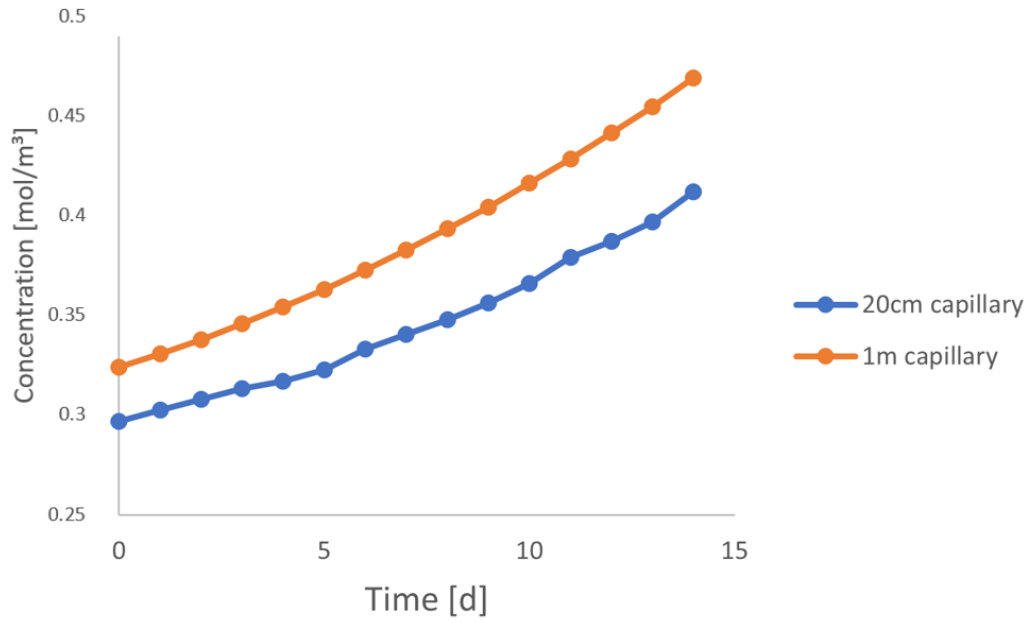
Figure 24: Oxygen Concentrations in the Mixed Species Capillary Biofilm Reactor Model with implementation of oxygen flux across the cultivation unit material, for two different capillary lengths. Concentrations are measured at the outlet of the cultivation unit
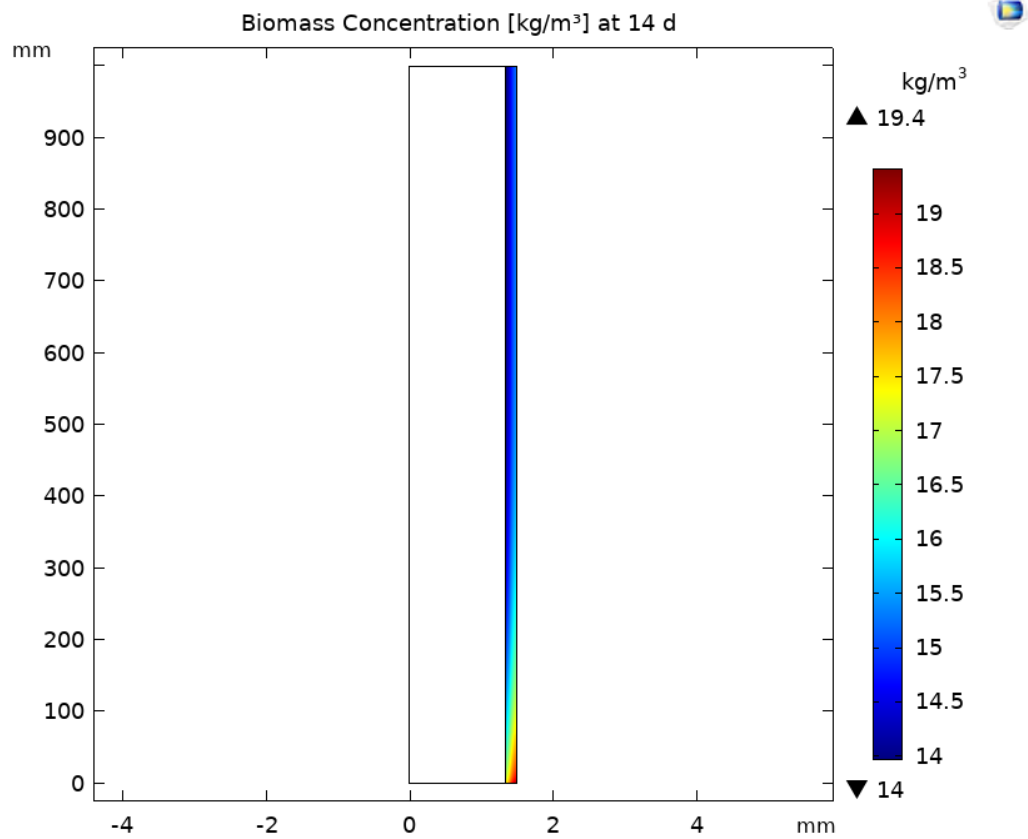
Figure 25: Distribution of the biomass in the biofilm of a 1m Mixed Species Capillary Biofilm Reactor Model on day 14 with included oxygen permeability of the cultivation unit material

In the reactor models the average biomass is calculated based on the biofilm volume. In Table 5 the amount of biomass in the 1m reactor seems to be lower than that in the 20cm reactor, however when calculating the weight of the biomass from the concentrations, it is $m_{1m,model} = 20.45$mg for the 1m capillary (volume $V_{1m} = 0.007$L) and $m_{20cm,model} = 4.49$mg for the 20cm capillary (volume $V_{20cm} = 0.0014$L). The total amount of biomass produced is higher in the longer capillary. Comparison of experimental results with model results in Table 5, shows that for the 20cm capillary the difference is almost 4 times lower than for the 1m capillary.

Table 5: Final biomass concentrations in experiments compared to final average biomass concentrations in oxygen permeable Mixed Species Capillary Biofilm Reactor models

Reactor Length	$c_{X,model}$[g/L]	$c_{X,experiment}$[g/L]
20cm	16.73	28.31 ±1.27
1m	15.26	60 ±35

For different reactor materials with different oxygen permeabilities, a scale up could lead to higher biomass production. Each setup should be evaluated individually, since a longer reactor with a high permeability does not necessarily lead to increased efficiency.

4.6 Impact of Growth Rates on Model Results

Growth rates of microorganisms are usually expressed through their maximum growth rates, in this work however literature values for cells in suspension resulted in biomass formations of up to 1000g/L, which is not realistic. Therefore, values more suitable for the described system were calculated using experimental data. However, these determined values are not maximum growth rates, since conditions to achieve the optimal growth are not provided in the experiments. The implementation of rates calculated based on data from Martin Schuster's Project Work resulted in a more realistic model outcome. The results however, were not identical with the experimental results. Therefore, different values for the maximum heterotrophic and phototrophic growth rates were tested and their effects on the model output evaluated. In order to assess how sensitive the response of the model is, with respect to uncertainties in the input, values for different parameters can be changed. This can also be a method to improve the performance of a model. Values for probable maximum growth rates in the biofilm described in this work were approached. For reasons of time deficiency, this was performed only on the gas impermeable reactor model with growth inhibition for a first analysis.

4.6.1 Model Sensitivity to Maximum Growth Rates

The phototrophic and heterotrophic growth rates $\mu_{max,pho}$ and $\mu_{max,het}$, respectively, are expected to have the biggest impact on the model output because they are directly linked to the growth rates of cells $r_{pho/het}$ and reaction rates are based on these rates $r_{pho/het}$. The values of these parameters were varied between the measured rates and the maximum growth rates known for cells in suspension.

The maximum phototrophic growth rate $\mu_{max,pho}$ was supposed to be varied between 0.008h^{-1} and 0.052h^{-1}, under the estimation that the growth rate for the heterotrophic strain is constant at $\mu_{max,het} = 0.02\text{h}^{-1}$. However, in addition to the calculated value of $\mu_{max,pho} = 0.008\text{h}^{-1}$ only $\mu_{max,pho} = 0.01\text{h}^{-1}$ and $\mu_{max,pho} = 0.02\text{h}^{-1}$ were tested, as for $\mu_{max,pho} = 0.03\text{h}^{-1}$ results for the biomass formation were too high (up to 252g/L) to be in a realistic range (see Fig. 28b compared to Fig. 28a). The changes in oxygen concentrations in the model for different growth rates are summarized in Fig. 26. For $\mu_{max,pho} = 0.008\text{h}^{-1}$ the slope is around 3.5 times higher than for $\mu_{max,pho} = 0.02\text{h}^{-1}$. The amount of O_2 increases with increasing growth rate due to more phototrophs performing oxygenic photosynthesis.

Fig. 27 shows the carbonate consumption in the gas impermeable reactor model for different values of $\mu_{max,pho}$. This consumption also increases with higher growth rates, as the amount of cells consuming carbonate increases as well.
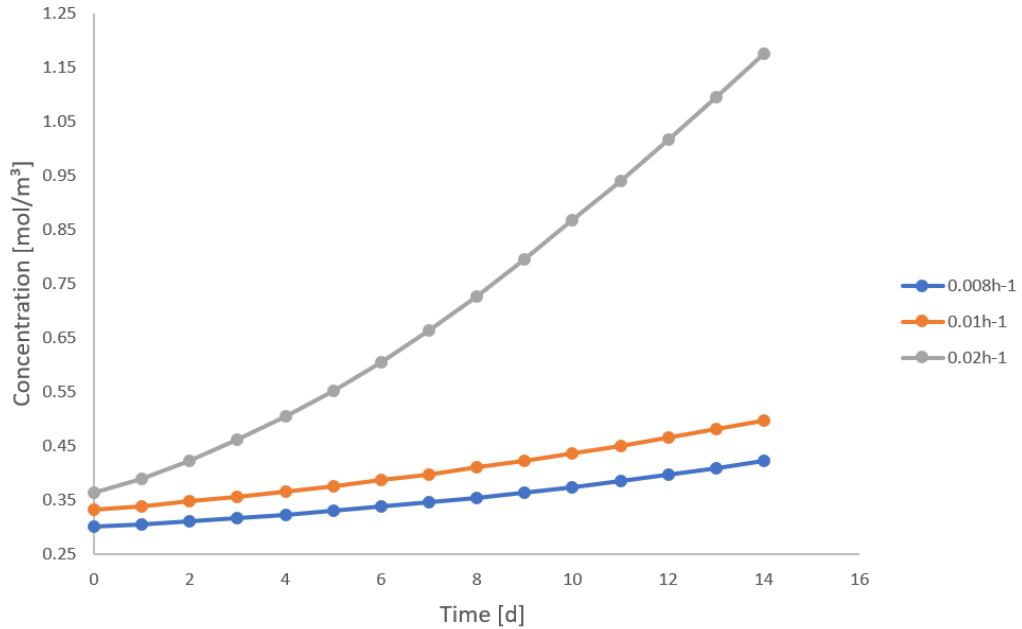
Figure 26: O_2 concentrations in the oxygen impermeable Mixed Species Capillary Biofilm Reactor Model for different values of the maximum phototrophic growth rate $\mu_{max,pho}$ and constant maximum heterotrophic growth rate $\mu_{max,het} = 0.02\text{h}^{-1}$

Figure 27: Carbonate consumption in an oxygen impermeable Mixed Species Capillary Biofilm Reactor Model for different values of the maximum phototrophic growth rate $\mu_{max,pho}$ and constant maximum heterotrophic growth rate $\mu_{max,het} = 0.02\text{h}^{-1}$

(a) Phototrophic biomass distribution on day 14 for $\mu_{max,het} = 0.02\text{h}^{-1}$ and $\mu_{max,pho} = 0.01\text{h}^{-1}$

(b) Phototrophic biomass distribution on day 14 for $\mu_{max,het} = 0.02\text{h}^{-1}$ and $\mu_{max,pho} = 0.03\text{h}^{-1}$

Figure 28: Phototrophic biomass distribution in a Mixed Species Capillary Biofilm Reactor Model on day 14 (without oxygen permeability of the cultivation unit material) for constant maximum hetertrophic growth rate $\mu_{max,het} = 0.02\text{h}^{-1}$ and two different phototrophic growth rates $\mu_{max,pho}$

The maximum heterotrophic growth rate $\mu_{max,het}$ was varied between 0.02h^{-1} and 0.5h^{-1}, under the estimation that the growth rate for the phototrophic strain is constant at $\mu_{max,pho} = 0.008\text{h}^{-1}$. Values tested were 0.05h^{-1} and 0.5h^{-1} in comparison with the calculated value $\mu_{max,het} = 0.02\text{h}^{-1}$. Fig. 29 shows the results concerning O_2 concentrations and Fig. 30 results concerning the carbonate consumption in the

reactor for these different parameter values. Having more heterotrophic cells producing CO_2 in the reactor leads to an increase in the carbonate concentration as the model does not differentiate between CO_2 and HCO^-_3. The increase in oxygen concentrations could be due to the availability of more carbon for the phototrophs which may result in an increased O_2 production. In Fig. 31, a slight increase between 31a and 31b, in the overall heterotrophic biomass concentration can be observed for $\mu_{max,het} = 0.5h^{-1}$ in comparison with the initial value $\mu_{max,het} = 0.02h^{-1}$. The number of heterotrophic cells towards the capillary outlet is higher than at the inlet, this could be due to the oxygen (which is consumed by heterotrophs) accumulation over the length of the cultivation unit.

Figure 29: O_2 concentrations in a Mixed Species Capillary Biofilm Reactor Model (without oxygen permeability of the cultivation unit material) for different values of the maximum heterotrophic growth rate $\mu_{max,het}$ and constant maximum phototrophic growth rate $\mu_{max,pho} = 0.008h^{-1}$

46
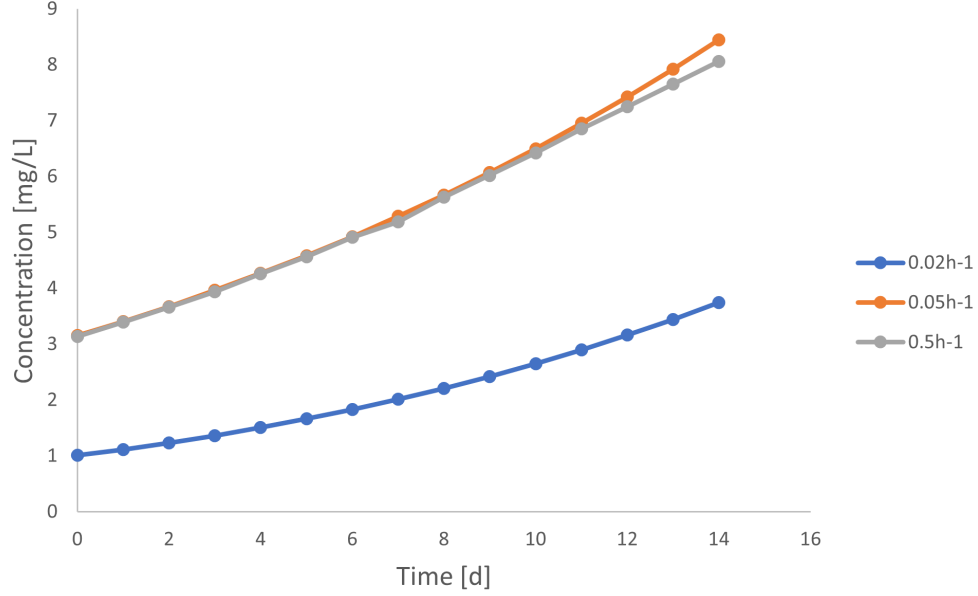
Figure 30: Carbonate consumption in a Mixed Species Capillary Biofilm Reactor Model (without oxygen permeability of the cultivation unit material) for different values of the maximum heterotrophic growth rate $\mu_{max,het}$ and constant maximum phototrophic growth rate $\mu_{max,pho} = 0.008\text{h}^{-1}$
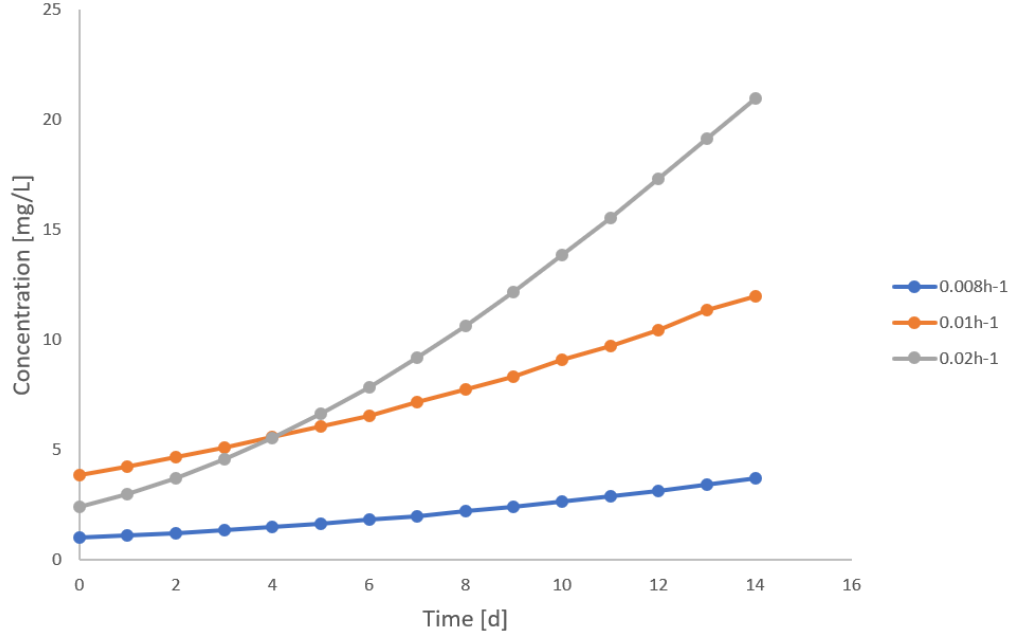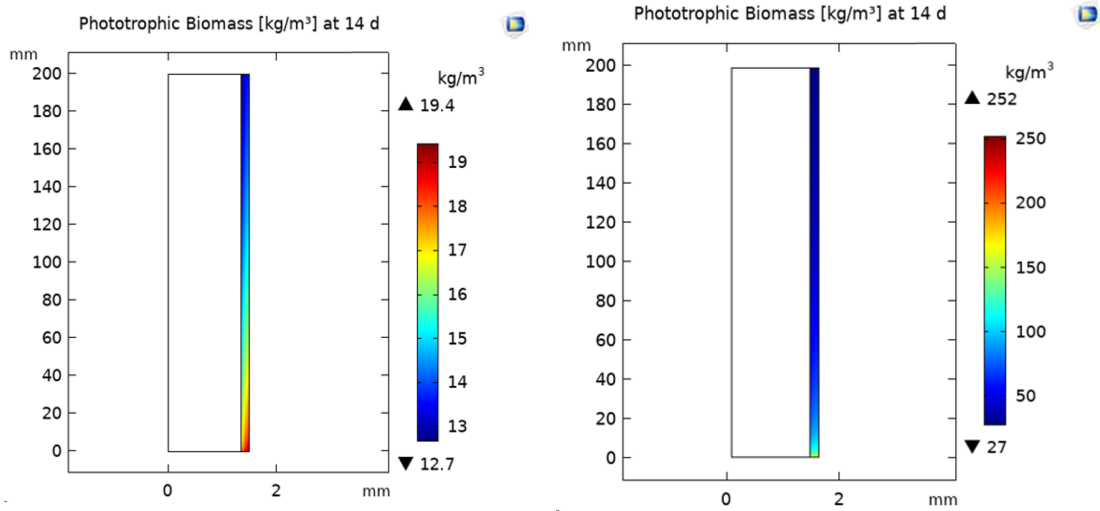

(a) Heterotrophic biomass distribution on day 14 for $\mu_{max,pho} = 0.008\text{h}^{-1}$ and $\mu_{max,het} = 0.02\text{h}^{-1}$

(b) Heterotrophic biomass distribution on day 14 for $\mu_{max,pho} = 0.008\text{h}^{-1}$ and $\mu_{max,het} = 0.5\text{h}^{-1}$
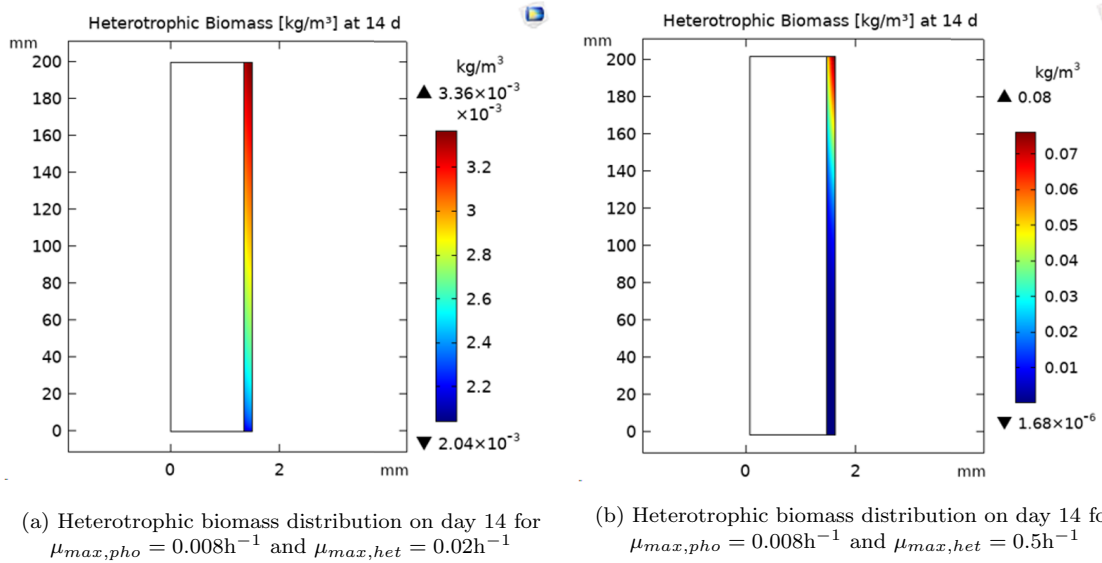
Figure 31: Heterotrophic biomass distribution in a Mixed Species Capillary Biofilm Reactor Model (without oxygen permeability of the cultivation unit material) on day 14 for constant maximum phototrophic growth rate $\mu_{max,pho} = 0.008\text{h}^{-1}$ and two different heterotrophic growth rates $\mu_{max,het}$

The influence of the maximum phototrophic growth rate on the oxygen concentrations in the model output is more significant than that of the maximum heterotrophic growth rate

4.6.2 Maximum Phototrophic Growth Rate Approached to Fit Experimental Results

Since the model developed in this work focuses on the influence of oxygen on cell growth, different values for $\mu_{max,pho}$ were tested, the O_2 concentrations were compared to experimental results and a value for $\mu_{max,pho}$ that delivers more accurate results was chosen.

For this purpose, model and experimental values of the oxygen concentration at a fixed time where compared. For the polystyrene reactor the experimental result on day 14 was $c_{O_2,experiment} = 0.671\text{mol/m}^3$. In the oxygen impermeable reactor the values for the O_2 concentration for $\mu_{max,pho} = 0.01\text{h}^{-1}$ and $\mu_{max,pho} = 0.02\text{h}^{-1}$ were $c_{O_2,model} = 0.498\text{mol/m}^3$ and $c_{O_2,model} = 0.970\text{mol/m}^3$, respectively. Therefore, to achieve the final experimental result, a value between these two growth rates had to be chosen. By iteration the maximum phototrophic growth rate was set to $\mu_{max,pho} = 0.0139\text{h}^{-1}$, for which the model result on day 14 was $c_{O_2,model} = 0.672\text{mol/m}^3$. Fig. 32 shows the oxygen concentration in the model and the experiment for low permeability. The model describes the system more accurately compared to results in section 4.4.1.
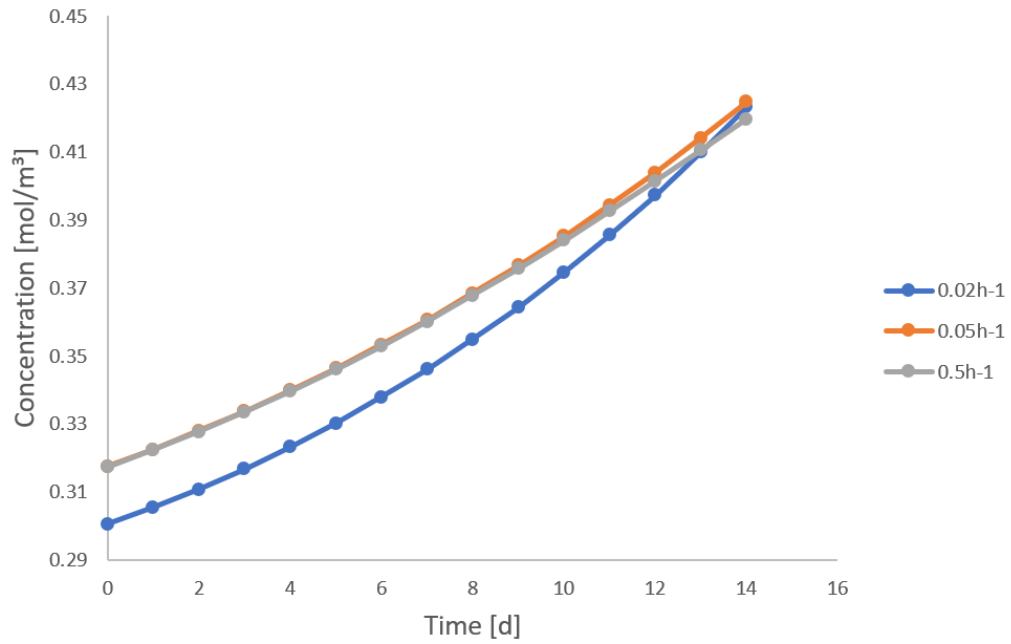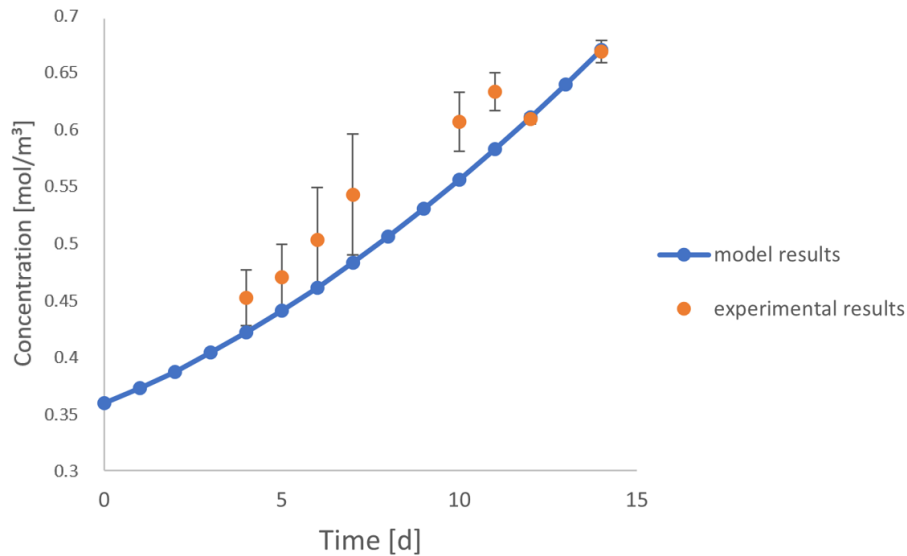

Figure 32: O_2 concentrations in the Mixed Species Capillary Biofilm Reactor Model (without oxygen permeability of the cultivation unit material) with $\mu_{max,pho} = 0.0139\text{h}^{-1}$ and $\mu_{max,het} = 0.02\text{h}^{-1}$ and in the experiment with polystyrene as reactor material

This $\mu_{max,pho} = 0.0139\text{h}^{-1}$ was implemented in the reactor model where oxygen permeability was included. Compared with an experimental results on day 14 from a silicone reactor $c_{O_2,experiment} = 0.376\text{mol/m}^3$, the model output was $c_{O_2,model} = 0.784\text{mol/m}^3$. This shows that the approached parameter fits only for the impermeable system and does not describe the permeable reactor more accurately.

5   Discussion

5.1   Oxygen Inhibition Reduces Biofilm Growth to Realistic Levels

The classification of inhibitors usually depends on the overall inhibition behavior observed, rather than the actual inhibition mechanism of the enzymes [13]. In this work only the phototrophic growth inhibition due to oxygen toxification was considered. Other inhibitions such as the one due to too high light intensities, or light limitation due to a too dense biofilm formation could be modeled. Comparing the growth rate of *Synechocystis* r_{pho} from a model with competitive oxygen inhibition and one with non-competitive oxygen inhibition, to the biomass formation observed in experiments, it is clear that the biological system can be described more accurately by a non-competitive inhibitor. Furthermore, the carbon source is provided through the medium in a sufficient amount, it would therefore not be possible for an O_2 inhibitor to compete with it.

Before the implementation of the inhibition term phototrophic microorganisms could grow unhampered, the biomass concentration was around 4 times higher than expected from experiments. The addition of such an inhibiting term reduced the amount of biomass formed to a realistic value that is in the same range as the experimental results. The gradual decrease in the growth rate is what causes the biomass to be dense at the inlet and less dense at the outlet. From experimental observations, the rate is expected to decrease with increasing oxygen concentrations, which is the case towards the outlet of the capillary where O_2 accumulates. It is also often observed that biomass forms at the beginning of the experiment, turns a yellowish color when the O_2 concentrations in the reactor increase and towards the outlet detachment of the biofilm often happens as well (mostly with polystyrene or glass reactors) [3, 39]. Detachment was not included in the model, therefore the biomass in the model is distributed over the whole biofilm and the amount produced towards the outlet of the capillary at the start of the simulation does not detach. In this work the biofilm density was defined as variable with a constant thickness and a changing amount of cells.

The stoichiometry of reactions also plays a major role in achieving a suitable model for the system. In this work they are based on the PHOBIA model, where the numbers were mathematically fitted to fulfill the mass balance. The biological system described and the goals of the two models are similar, thus these stoichiometric factors could be used as a good approach to describe the system in this work. This of course lowers the accuracy of results, as the described systems are not identical,

which leads to a qualitative model. For higher accuracy the stoichiometric factors corresponding to the biological processes in the system could be determined.

5.2   Oxygen Permeability of the Reactor Influences Oxygen Concentrations in the Biofilm

The geometry of the reactor material was chosen to be omitted in this model. The mass transport mechanisms related with different materials were described through a flux into the surrounding environment. In this work only the mass transport of oxygen through the reactor material was modeled. This approach does not increase the complexity of the model as the addition of an extra layer would. The driving force behind this mechanisms is the concentration gradient and the partial O_2 pressure on either side of the boundary. The partial pressure in the membrane was assumed to be the same as in the medium. The determination of the O_2 concentration in the membrane would increase the accuracy of the results.

One drawback is that, in order to simulate different reactor materials, values for their oxygen permeability need to be known. It has also yet to be investigated, in what form the oxygen travels through different membranes. This could differ from one material to another. The pore-flow model could be used, where the membrane is considered microporous and the fluid transport happens through these capillary pores under pressure [40]. Another approach could be the application of the solution-diffusion mechanism model, where oxygen dissolves into the membrane and then diffuses through it [41]. This work focuses on silicone as reactor material, which is a nonporous rubber [42], therefore the solution-diffusion model was applied. The model developed in this work is restricted to oxygen permeability. Mass transport mechanisms concerning for example CO_2 and other gases was not included, therefore results delivered by the model have a limited accuracy.

In this work the oxygen concentrations in the reactor play a major role, as the effects of oxidative stress, caused by high O_2 levels, on cell growth was primarily investigated. Even though the permeable reactor has lower oxygen concentrations, the curve in Fig. 16 seems to have a steeper slope in the concentration increase. This could be due to the higher activity of phototrophs compared to their hampered oxygen production in the impermeable reactor. Comparing the experimental results with results from the model for an oxygen impermeable system, the concentrations increase with a higher rate in the experiment, while in the model there is a limit to this increase and the concentrations reach a plateau before the experimental maximum is attained. This could be due to the chosen model to describe the growth inhibition or to the parameters describing the growth and oxygen production rates.

However, the reason behind this is not yet known. For an oxygen permeable system, concentrations in the model are higher than in the experiments, this could either be due to a low permeability or to the growth and oxygen production rates implemented. The O_2 concentrations in reality reach a maximum and do not rise further which is not the case in the model, where concentrations continue to increase. The reason behind these model deviations have to be further investigated. Here the oxygen production rate could need adjustment as well as the chosen approach to describe the reactor permeability. Furthermore, it has to be taken into consideration that in reality these systems are not only permeable for oxygen but also for other gases. Therefore, model results cannot perfectly fit experimental results when the rest of the mass transport mechanisms is not included. For the oxygen concentrations this could be neglected for a first result analysis as the CO_2 permeability is not expected to affect the phototrophic cell activity since their need in carbon is covered through the amount provided as carbonate in the medium. However, an impact on the overall behavior of microorganisms is not excluded. Therefore, the carbonate concentrations from the model were not compared to the experimental results. Only model results from both reactor types were compared, the higher carbonate consumption in the oxygen permeable reactor could be due to the increased phototrophic activity which is not as hampered by the O_2 levels as in the oxygen impermeable reactor. The oxygen permeability of the reactor material helped relieve oxidative stress and increase the cell activity in the biofilm, resulting in lower O_2 levels and a higher carbonate consumption.

5.3 Reactor Permeability Influences Biofilm Growth

The biofilm thickness was set to a maximum and assumed to be constant. The approach of using a variable density was to simplify the model and not to implement a geometry deformation linked to the biofilm growth. From the beginning, reactors are inoculated with a higher concentration of phototrophs than heterotrophs, and heterotophic cells only consume the produced substrate and O_2, their carbon source is therefore limited. Through the run of the experiments as well as the simulations, the phototrophic cell activity dominates as their concentration is never below 63%. Therefore, the biomass distribution in the biofilm is mostly determined by the phototrophs.

The amount of biomass produced in the oxygen permeable reactor model is higher than in the oxygen impermeable reactor model, this is consistent with the experimental observations. With the phototrophs being the biggest part of the biofilm, their increased growth increases the overall biomass concentration. More phototrophic

cells contribute to more substrate production on which heterotrophs feed, this leads to an increase in their cell numbers as well. Due to the transport of O_2 out of the reactor, the oxygen concentrations decrease and the phototrophic growth inhibition increases with a slower rate, resulting in a more dense coverage of the capillary with biomass than in the oxygen impermeable reactor model. The model developed in this work seems to provide a more accurate description of a system with low oxygen permeability concerning the biomass concentrations. The difference in results between the silicone reactor and the oxygen permeable reactor model could be due to the inaccuracy of the mass transport description. Nevertheless, growth behavior can be analyzed on a qualitative level.

5.4 Scale-Up Impact on Oxygen Concentrations and Biomass Production

Having selected a suitable reactor material that helps reduce oxidative stress, different lengths and their impact on oxygen accumulation and biomass production can be tested. Doing this for a material (example: polystyrene) where cell growth is already strongly inhibited in a 20 cm capillary would not lead to new findings, therefore the model comparable with a silicone reactor was tested for two different lengths. The oxygen concentrations at the outlet of the capillary are higher in the longer capillary since O_2 accumulates despite the permeability. Testing different reactor lengths enables the determination of the point where the accumulated oxygen reaches the toxic level and cell growth is inhibited.

The comparison of biomass concentrations from experimental data with model results constitutes a challenge, since the determination of the total biomass in the biofilm from the model was not yet possible. Having a longer capillary the total amount of biomass produced is around 5 times higher, however it is distributed over a volume that is around 5 times larger than in the 20cm capillary. Therefore, the average biomass concentration is around 9% lower. While in the 20cm capillary model, the part where the biomass concentration is the lowest is around 20mm from the outlet, in the 1m capillary reactor it makes up more than half of the reactor. This shows that the oxygen accumulation increases with the increasing length of the reactor. In a more permeable reactor this part could be reduced even further, however it should be taken into consideration that the permeability in this model only includes oxygen. For a more accurate system representation, the mass transport of other gases out of the reactor should be considered.

5.5 Maximum Growth Rates can be Approached Through Iteration

In order to achieve the maximum growth rate μ_{max} for a microorganism, certain conditions need to be provided, which was not the case in this work. Unfortunately, data on maximum growth rates in biofilms is scarce and therefore determined results are not easy to compare. Maximum growth rates in biofilms could be lower than in suspensions, due to the fact that with the continuous mixing in suspension, cells have a more direct and easy access to nutrients, which is not the case in biofilms, where nutrients have to diffuse through gel-like layers. This does not exclude the possibility that maximum growth rates could be the same for cells independent from the system they are grown in, as the species remain the same. Here again the bottleneck in data on cell growth in biofilms, constitutes a challenge to obtain representative parameters. In this work the calculated values for $\mu_{max,pho}$ and $\mu_{max,het}$ are not maximum values, as the conditions under which the cells were cultivated do not correspond to those needed for optimal growth. However, these values seem to provide a more accurate description of the biological processes taking place in the system than values from literature for suspended cells.

Different values between the calculated maximum growth rates and the rates known from literature were tested, and model results (oxygen, carbonate and biomass concentrations) were compared to experimental results. In Figures 26, 27, 29 and 30, the initial concentrations are not the same for different growth rates. This could be due to the fact that values were analyzed at the outlet of the capillary. Also, results for the time dependent study were computed based on a stationary study, therefore depending on the activity rate of cells, processes could have already taken place and concentrations within the reactor changed.

The effect of the heterotrophic growth on the model output is smaller compared to that of the phototrophic growth. This could be due to the fact that the amount of heterotrophic cells in the reactor is smaller and their growth is strongly limited by the available substrate, which is the amount of degraded inactive cells. Therefore the species they consume and produce are in a low range and processes related to phototrophic microorganisms "take over" the system. The growth of heterotrophic organisms on degraded inactive cells might not be fully biologically correct, however for a first approach of modelling without considering the production of EPS and polysaccharides for the heterotrophs to feed on, this seems a god way to describe an undetermined system.

In order to overcome the gap in data concerning biofilms, growth rates could be approached by testing different values (by performing a Parametric Sweep in COMSOL

for example) and comparing the model output to experimental results. In this work the most basic biological processes were implemented, however there are still many effects and processes that are not taken into consideration. For example the production of enzymes, proteins, EPS etc. were not included as well as biofilm growth (geometrically) and detachment. Another observable difference between the experimental setup and the model is that the light in the model penetrates the capillary from all sides, whereas in the experiment the light source is situated on top of the cultivation unit. To try and minimize the effects of light attenuation, the tubes were mounted on a white surface, for maximal reflection. In reactors with polystyrene for example, where the biofilm formed is not very dense, this effect could be negligible. However, with silicone as reactor material the effects of light attenuation could be bigger due to the dense biomass formation in the tubes.

Since the mathematical model will never be a perfect description of the biological system, some differences could be compensated by the iteration of parameters. However, this approach should be handled carefully, since the risk of losing sight of possible model deficiencies is high. In this work, a value for the maximum phototrophic growth rate was approached specifically for the oxygen impermeable reactor model. Implementing this rate into the oxygen permeable reactor model did not result in a more accurate description of the system. This makes it clear that, in addition to different parameter values, different combinations of them should be tested to achieve an optimal fit.

6 Conclusion

In conclusion, the model developed in this work to describe a Mixed Species Capillary Biofilm Reactor, delivered realistic results concerning oxygen and carbonate concentrations within the reactor, as well as the amount of biomass produced. The implementation of parameters and kinetics determined specifically for the described system led to model results that were in the same range as experimental results. The addition of an inhibition term for the phototrophic growth resulted in the limitation of the cell number increase and delivered a distribution of the biomass in the biofilm that is comparable to what was observed in experiments. The oxygen permeability was described through an oxygen flux out of the reactor, different materials could be modeled by implementing the corresponding permeability. This resulted in the decrease of the oxygen concentration towards the outlet of the capillary, in the increase of the biomass and with that the increase of the carbonate consumption within the reactor. The determination of specific maximum growth rates for the modeled system kept the model results from reaching unrealistic levels, however, these rates could not be described as maximum values. They were calculated from reactor setups that did not provide the optimal growth conditions. Maximum growth rates could be approached but the interaction of these kinetics and other parameters has to be taken into consideration to achieve an optimal fit for all reactor setups. In this work, with the focus on O_2 concentrations within the reactor, a maximum phototrophic growth rate for an impermeable reactor model was approached, since the impact of phototrophs on the oxygen levels was more significant than that of the heterotrophs. This however, led to a less accurate description of the permeable reactor.

Finally, results are sufficiently accurate to provide the possibility to test different reactor permeabilities (simulating different materials), reactor lengths, flow rates and light intensities in the future. Different combinations of these conditions can also be evaluated. However, the model does not provide quantitative results.

7   Summary

In this work a mathematical model for a Mixed Species Capillary Biofilm Reactor was developed and implemented in COMSOL. The model is based on the kinetic and metabolic PHOBIA model created by Wolf and others in 2007 [11]. It is a description of a mixed species biofilm (where *Synechocystis* sp. PCC 6803 is grown in combination with *Pseudomonas taiwanensis* VLB120) attached to the inner wall of a tube, with a nutritional medium flowing through. The basic biological processes included in this model were cell growth, inactivation and decay, diffusion of carbonate, substrate and oxygen within the reactor, as well as the flux of oxygen out of it. Phototrophic growth inhibition due to oxygen toxification was included as well.

Parameters, kinetics and initial conditions were determined from experiments and implemented to achieve a realistic description and model results in the right range. However, due to the complexity of the biological system many processes had to be excluded and many assumptions and simplifications had to be made. Therefore, model results still show some deviations from the experimental results.

The impact of the inhibiting effect of high oxygen concentrations within the reactor on biofilm development were investigated. This resulted in a biomass distribution in the biofilm that resembled the experimental observations, with a higher cell density at the cultivation unit inlet compared to the outlet.

The effects of the oxygen permeability of the reactor material on oxygen and carbonate concentrations and on cell growth were analyzed. For a model with implemented oxygen flux, two reactor lengths were compared and their effects on O_2 accumulation and biofilm growth were analyzed. Implementing the oxygen flux across the reactor material wall resulted in the decrease of the O_2 levels in the biofilm and with that an increased phototrophic cell activity, producing more biomass and consuming more carbonate.

The method of approaching parameters that were not determined experimentally (example the maximum growth rates of cells in biofilms) to achieve a more accurate system description was shortly tested. After concluding that the maximum phototrophic growth rate $\mu_{max,pho}$ has a bigger impact on the oxygen concentrations in the reactor than the heterotrophic growth rate, and with the focus of the model being on the O_2 accumulation, a value for $\mu_{max,pho}$ in the impermeable model was approached. This led to model results that are closer to experimental results for the impermeable reactor model, but created a larger gap for results in the permeable reactor model. This shows that in order to achieve an optimal fit, different parameter values and combinations as well as their relationships and impact on each other should be investigated.

8 Outlook

Due to the complexity of the biological system, the model developed in this work is based on many assumptions and simplifications. For an even better description of the system, it might be of interest to include other processes, such as the excretion of EPS or the consumption of nitrate and phosphate by microorganisms. The heterotrophic growth could be described more accurately by the implementation of polysaccharides and EPS excretion, on which they feed in reality. In future studies the growth and decay of cells within the biofilm could be further investigated to obtain representative data on such mixed species biofilms. The determination of more accurate model kinetics, such as growth and inactivation rates in biofilms, could also contribute to a closer description of the biological system. The relationships between different parameters and their effects on the model output has yet to be investigated.

To investigate the influence of light and light attenuation on cell behavior in the model, a 3-Dimensional model could be created. In experiments is has been observed that too high intensities could lead to cell inactivation, cell behavior in nature-like conditions could be investigated through the simulation. Light coverage of different surface areas of the capillary, different intensities and maybe different shapes of the tubes could be investigated.

Another difference between the model and the described system is that the change in geometry due to the biofilm growth was neglected in this work. Depending on the aim of the model, the geometry deformation could be implemented, in addition to the detachment events observed in experiments. This could deliver more accurate results concerning the biomass production in the reactor and the effects of different medium flow rates could be investigated.

The stoichiometry of the modeled reactions was a challenge in this work, the stoichiometric factors used in the final version of the model were taken from the PHOBIA Model. The similarity of the biological system described in the PHOBIA Model to the system described in this work enabled the attainment of realistic results. However, for an optimal mathematical description of the reactions, these factors should be determined specifically for the modeled system.

Due to the focus of this work on the O_2 accumulation in the reactor and the oxygen flux out of it, results concerning the carbonate and substrate consumption and production as well as the biomass formation are less accurate and the related processes require further adjustment. A major restriction of this model is the reduction of the gas permeability of reactor materials to their oxygen permeability. The flux of CO_2 could have an important effect on cell growth. What also needs to be taken into

consideration is the permeability of materials to other substances. If a reactor is oxygen permeable it is probably also hydrogen permeable. This would constitute a major problem if the aim of the reactor is the H_2 production through cyanobacteria. The same problem could occur during the production of value-added chemicals or due to the presence of toxic substances within the reactor.

References

[1] Alchetron. Synechocystis. `https://alchetron.com/Synechocystis#`
`synechocystis-4ccc7e63-5763-491e-8ecb-d1a29ff3a43-resize-750.`
`jpeg`, accessed November 01, 2021.

[2] Babu Halan, Igor Vassilev, Karsten Lang, Andreas Schmid, and Katja Buehler.
Growth of *Pseudomonas taiwanensis* vlb120δc biofilms in the presence of *n*-butanol. *microbial biotechnology*, 10:745–755, 2016.

[3] A. Hoschek, I. Heuschkel, A. Schmid, B. Bühler, R. Karande, and K. Bühler.
Mixed-species biofilms for high-cell-density application of *Synechosystis* sp. pcc
6803 in capillary reactors for continuous cyclohexane oxidation to cyclohexanol.
Bioresource technology, 282:171–178, 2019.

[4] Ana C. Barros, Ana L. Goncalves, and Manuel Simoes. Microalgal/cyanobacterial biofilm formation on selected surfaces: the effects of surface physicochemical properties and culture media composition. *Journal of Applied Phycology*,
31:375–387, 2019.

[5] Levi Straka. Light-dependent growth kinetics and mathematical modeling of
Synechocystis sp. pcc 6803. *A dissertation Presented in Partial Fulfillment of
the Requirements for the Degree Doctor of Philosophy*, 2017.

[6] Debajyoti Dutta, Debojyoti De, Surabhi Chaudhuri, and Sanjoy K Bhattacharya. Hydrogen production by cyanobacteria. *Microbial Cell Factories*,
4, 2005.

[7] Bhavish Patel, Bojan Tamburic, Fessehaye W. Zemichael, Pongsathorn
Dechatiwongse, and Klaus Hellgardt. Algal biofuels: A credible prospective?
ISRN Renewable Energy, 2012.

[8] I. Heuschkel, A. Hoschek, A. Schmid, B. Bühler, R. Karande, and K. Bühler.
Mixed-trophies biofilm cultivation in capillary reactors. *MethodsX*, 6:1822–1831,
2019.

[9] Chang Kenneth. Visions of life on mars. *The New York Times*, 2016.

[10] Douglas Harper. Online etymology dictionary. 2013.

[11] Gundula Wolf, Cristian Picioreanu, and Mark C.M. van Loosdrecht. Kinetic
modeling of phototrophic biofilms: The phobia model. *Biotechnology and Bioengineering*, 97:1064–1079, 2007.

[12] Antonio Blanco and Gustavo Blanco. Medical biochemistry. 1:126–152, 2017.

[13] Khan Academy. Enzyme regulation. `https://www.khanacademy.org/science/ap-biology/cellular-energetics/environmental-impacts-on-enzyme-function/a/enzyme-regulation`, accessed October 08, 2021.

[14] Madigan M. and Martinko J. Brock biology of microorganisms. 2005.

[15] Jan-Ulrich Kreft, Cristian Picioreanu, Julian W.T. Wimpenny, and Mark C.M. van Loosdrecht. Individual-based modelling of biofilms. *Microbiology*, 147:2897–2912, 2001.

[16] Rohan Karande, Babu Halan, Andreas Schmid, and Katja Buehler. Segmented flow is controlling growth of catalytic biofilms in continuous multiphase microreactors. *Biotechnology and Bioengineering*, 111:1831–1840, 2014.

[17] Babu Halan, Katja Buehler, and Andreas Schmid. Biofilms as living catalysts in continuous chemical syntheses. *Trends in Biotechnology*, 30:453–465, 2012.

[18] Christian David, Katja Bühler, and Andreas Schmid. Stabilization of single species *Synechocystis* biofilms by cultivation under segmented flow. *J Ind Microbial Biotechnol*, 42:1083–1089, 2015.

[19] Bettina Rosche, Xuan Zhong Li, Bernhard Hauer, Andreas Schmid, and Katja Buehler. Microbial biofilms: a concept for industrial catalysis? *Trends in Biotechnology*, 27:636–643, 2009.

[20] M. Henze, C. P. L. Grady Jr, W. Gujer, G. v. R. Marais, and T. Matsuo. Activated sludge model no. 1. *Scientific and Technical Reports*, 1, 1987.

[21] Cristian Picioreanu, Mark C.M. van Loosdrecht, and Joseph J. Heijnen. Modelling and predicting biofilm structure. *Cambridge University Press*, pages 129–166, 2000.

[22] O. Wanner and W. Gujer. A multispecies biofilm model. *Biotechnology and Bioengineering*, 28:314–328, 1986.

[23] O. Wanner and P. Reichert. Mathematical modeling of mixed-culture biofilms. *Biotechnology and Bioengineering*, 49:172–184, 1996.

[24] James D. Bryers and F. Drummond. Local macromolecule diffusion coefficients in structurally non-uniform bacterial biofilms using fluorescence recovery after photobleaching (frap). *John Wiley & Sons, Inc*, pages 462–473, 1998.

[25] COMSOL. Finite element method. `https://www.comsol.de/multiphysics/fea-software?parent=finite-element-method-042-62-22`, accessed September 25, 2021.

[26] Bastian E. Rapp. Microfluidics: Modelling, mechanics and mathematics. *Micro and Nano Technologies*, pages 137–188, 2017.

[27] COMSOL Multiphysics. Diffusion, a mass transfer phenomenon. `https://www.comsol.de/multiphysics/what-is-diffusion?parent=fluid-flow-heat-transfer-and-mass-transport-0402-392`, 2018 (accessed July 4, 2021).

[28] J.D. Seader, Ernest J. Henley, and D. Keith Roper. Separation process principles: Chemical and biochemical operations. *ISBN 978-0-470-48183-7*, 3rd Edition, 2011.

[29] G.C. Okpokwasili and C.O. Nweke. Microbial growth and substrate utilization kinetics. *African Journal of Biotechnology*, 5:305–317, 2005.

[30] Myer L. Coval. Analysis of hill interaction coefficients and the invalidity of the kwon and brown equation. *The Journal of Biological Chemistry*, 245:6335–6336, 1970.

[31] P. Reichert, M. Henze, W. Rauch, P. Shanahan, L. Somlyody, and P.A. Vanrolleghem. River water quality model no 1. *Scientific and Technical Reports*, 12:129–166, 2001.

[32] Z. Hu and D. Grasso. Water analysis, chemical oxygen demand. *Encyclopedia of Analytical Science*, 2:325–330, 2005.

[33] PyroScience GmbH. Sensing principle: Optical oxygen sensors. `https://www.pyroscience.com/en/products/theory/optical-oxygen-sensors`, accessed July 06, 2021.

[34] Binh T. Nguyen and Bruce E. Rittmann. Effects of inorganic carbon and ph on growth kinetics of *Synechocystis* sp. pcc 6803. *Algal Research*, 2016.

[35] Hatta Tatsuo. Le chatelier principle. *The New Palgrave: A Dictionary of Economics*, 3, 1987.

[36] Zavrel T., Ocenasova P., and Cerveny J. Phenotypic characterization of *Synechocystis* sp. pcc 6803 substrains reveals differences in sensitivity to abiotic stress. *Plos One*, 2017.

[37] VAAM Vereinigung für Allgemeine und Angewandte Mikrobiologie. Wie wiegt man ein bakterium? `https://vaam.de/infoportal-mikrobiologie/kurze-frage/wie-wiegt-man-ein-bakterium/`, accessed Oktober 25, 2021.

[38] Jean Tague, Jamshid Beheshti, and Lorna Rees-Potter. The law of exponential growth: Evidence, implications and forecasts. *Library Trends*, pages 125–149, 1981.

[39] Ingeborg Heuschkel, Rakesh Dagini, Rohan Karande, and Katja Buehler. The impact of glass material on growth and biocatalytic performance of mixed-species biofilms in capillary reactors for continuous cyclohexanol production. *Frontiers in Bioengineering and Biotechnology*, 8, 2020.

[40] D. Bhattacharyya, M. Jewtitch, and J.T. Schrodt. Prediction of membrane separation characteristics by pore distribution measurements and surface force-pore flow model. *Chemical Engineering Communications*, pages 111–128, 2007.

[41] Ahmad Fauzi Ismail, Tutuk Djoko Kusworo, Azeman Mustafa, and Hasrinah Hasbullar. Understanding the solution-diffusion mechanism in gas separation membrane for engineering students. *Proceedings of the 2005 Regional Conference on Engineering Education*, pages 155–159, 2005.

[42] Pavel Kuban and Petr Bocek. Chapter 8: Green-membrane extraction. *The Application of Green Solvents in Separation Processes*, pages 217–251, 2017.

[43] I. Heuschkel, A. Hoschek, A. Schmid, B. Bühler, R. Karande, and K. Bühler. Data on mixed trophies biofilm for continuous cyclohexane oxidation to cyclohexanol using *Synechosystis* sp. pcc 6803. *Data in Brief*, 25, 2019.

[44] F. Garcia-Pichel. Cyanobacteria. *Encyclopedia of Microbiology*, 3, 2009.

[45] W. L. Robb. Thin silicone membranes- their permeation properties and some applications. *Materials in Biochemical Engineering*, 146:119–137, 1968.

[46] Amel Latifi, Marion Ruiz, and Cheng-Cai Zhang. Oxidative stress in cyanobacteria. *FEMS Microbial Rev*, 33:258–278, 2008.